# DEVELOPMENTAL AND EVOLUTIONARY COMPARATIVE ANALYSIS OF A REGULATORY LANDSCAPE IN MAMMALS AND BIRDS

Aurélie Hintermann[1], Isabel Guerreiro[1,a], Christopher Chase Bolt[2], Lucille Lopez-Delisle[2], Sandra Gitto[1], Denis Duboule[1,2,3,#] and Leonardo Beccari[1,b]

**Short title: Regulation evolution at the *HoxD* locus**

Keywords: Chromatin topology, TAD, enhancers, evolution, gene regulation, development, teguments, placodes

[1]Department of Genetics and Evolution, University of Geneva, 30 quai Ernest-Ansermet, 1211, Geneva, Switzerland.
[2]School of Life Sciences, Federal School of Technology (EPFL), 1015 Lausanne, Switzerland.
[3]Collège de France, 75005 Paris, France.

[a]Present address: Oncode Institute, Hubrecht Institute-KNAW and University Medical Center Utrecht, Utrecht, The Netherlands.

[b]Present address: Institut Neuromyogène. CNRS UMR 5310, INSERM U1217, University of Lyon, Lyon, France.

[#]Corresponding author

Denis Duboule
Denis.Duboule@unige.ch

**ABSTRACT**

Modifications in gene regulation during development are considered to be a driving force in the evolution of organisms. Part of these changes involve rapidly evolving *cis*-regulatory elements (CREs), which interact with their target genes through higher-order 3D chromatin structures. However, how such 3D architectures and variations in CREs contribute to transcriptional evolvability remains elusive. During vertebrate evolution, *Hox* genes were redeployed in different organs in a class-specific manner, while maintaining the same basic function in organizing the primary body axis. Since a large part of the relevant enhancers are located in a conserved regulatory landscape, this gene cluster represents an interesting paradigm to study the emergence of regulatory innovations. Here, we analysed *Hoxd* gene regulation in both murine vibrissae and chicken feather primordia, two mammalian- and avian-specific skin appendages which express different subsets of *Hoxd* genes, and compared their regulatory modalities with the regulations at work during the elongation of the posterior trunk, a mechanism highly conserved in amniotes. We show that in the former two structures, distinct subsets of *Hoxd* genes are contacted by different lineage-specific enhancers, likely as a result of using an ancestral chromatin topology as an evolutionary playground, whereas the regulations implemented in the mouse and chicken embryonic trunk partially rely on conserved CREs. Nevertheless, a high proportion of these non-coding sequences active in the trunk appear to have functionally diverged between the two species, suggesting that transcriptional robustness is maintained despite a considerable divergence in CREs' sequence, an observation supported by a genome-wide comparative approach.

## INTRODUCTION

Changes in the spatial and temporal regulation of genes critical for developmental processes have greatly contributed to the evolution of animal morphologies (see for example (Carroll, 2008; Rebeiz et al., 2015). The expression of such genes is generally modulated by combinations of *cis*-regulatory elements (CREs), short DNA sequences enriched for transcription factor binding sites, which tend to evolve more rapidly than the genes they control (Edwards et al., 2013; Long et al., 2016; Spitz and Furlong, 2012). CREs can be spread over large distances around the gene(s) they regulate, which gives to the spatial organization of chromatin a particular importance. Indeed, the existence of such 'regulatory landscapes' (Spitz et al., 2003) implies that enhancer-promoter interactions involve spatial proximity, which is generally thought to occur through large chromatin loops (Rao et al., 2014).

The extent of regulatory landscapes often correspond to Topologically Associating Domains (TADs) (Andrey et al., 2013; Harmston et al., 2017), which were defined as chromatin domains where the probabilities of interactions, as measured by chromosome conformation capture (Belton et al., 2012), are higher than when compared to the neighbouring regions (Dixon et al., 2012; Nora et al., 2012; Sexton et al., 2012). The distribution of TADs tends to be conserved in various vertebrate species, a phenomenon likely associated with regulatory constraints exerted by the complex and pleiotropic regulations found around many vertebrate developmental genes. Such domains, where many interactions might occur, were proposed to form particular chromatin niches, rich in various DNA-binding proteins and where the evolutionary emergence of novel regulatory sequences could be favoured due to the presence of both a pre-existing scaffold and appropriate co-factors (see (Darbellay and Duboule, 2016a). While genomic rearrangements altering the structure of TADs were reported to impact proper gene regulation during development, sometimes leading to genetic syndromes (e.g. (Bolt et al., 2021a; Bompadre and Andrey, 2019; Lupianez et al., 2015), in most cases, these rearrangements also affected enhancer-promoter spatial relationships, which makes a causal assessment difficult.

Genome-wide analyses carried out in different species, comparing DNA sequence conservation, TAD organization, or some epigenetic modifications, have started to reveal some of the molecular mechanisms underlying both the evolution of gene regulation and, by extension, the modification of species-specific traits. However, integrated functional approaches are required to better understand how changes in chromatin architecture and modifications in CREs may influence the evolvability and the robustness of gene transcription. To try to address such questions, we have used the *HoxD* locus as a paradigm of pleiotropic regulation of a multi-gene family, with a strong impact both on the control of important developmental steps, and on the emergence of evolutionary novelties. The *HoxD* cluster contains a series of genes in *cis*, which encode transcription factors that are expressed in different combinations across several embryonic structures. The cluster is flanked by two large TADs, each one matching a gene desert highly enriched in CREs (Darbellay and Duboule, 2016a). These two TADs are separated by a boundary region which is localized within the

89 cluster, close to its centromeric extremity (Andrey et al., 2013; Rodriguez-Carballo et al., 2017). The telomeric
90 TAD comprises a large number of enhancers controlling transcription of various *Hoxd* genes in most of the
91 tissues where HOX proteins operate (Andrey et al., 2013; Darbellay et al., 2019; Delpretti et al., 2013;
92 Guerreiro et al., 2016; Schep et al., 2016). In contrast, the centromeric TAD contains enhancers specific for
93 terminal structures such as digits or external genitals (Amândio et al., 2020; Montavon et al., 2011).

94 Amongst the many tissues where *Hoxd* genes exert a function are embryonic primordia of different
95 skin derivatives, including those of mammary glands, vibrissae and pelage hairs of mammals as well as those
96 of chicken feathers (Kanzler et al., 1997, 1994; Reid and Gaunt, 2002; Reynolds et al., 1995; Schep et al.,
97 2016)(Fig. 1). Despite the fact that these ectodermal structures share common developmental mechanisms and
98 gene regulatory networks such as the *Wnt*, EDA and BMP signaling pathways (Biggs and Mikkola, 2014;
99 Dhouailly et al., 2019; Di-Poï and Milinkovitch, 2016; Pantalacci et al., 2008; Wu et al., 2004), each type of
100 primordium expresses different subsets of contiguous *Hoxd* genes. Since the specific topological organization
101 of the *HoxD* locus can be observed in fishes (Acemel et al., 2016) (see Fig. S1A), it likely predates the
102 emergence of hairs and feathers during amniote evolution (Dhouailly, 2009; Wu et al., 2004). For this reason,
103 these organs represent valuable models to understand how CRE evolution within a pre-existing chromatin
104 architecture could lead to the implementation of new gene-specific expression patterns. In contrast, the general
105 organization of *Hoxd* gene expression along the main embryonic body axis is overall maintained across
106 vertebrate species, in spite of the low sequence conservation observed, raising the question as to how evolving
107 *Hox* clusters could maintain globally similar transcriptional outputs.

108 In this study, we addressed these issues by taking a comparative look at a well-defined regulatory
109 landscape, positioned telomeric to the *HoxD* gene cluster, in mammals and in birds. These two syntenic regions
110 contain CREs involved either in the same regulatory tasks, or controlling regulatory aspects specific to each
111 taxon. In the latter context, we characterized *Hoxd* gene regulation in the mouse-specific vibrissae primordia
112 (VPs) and in the chicken-specific feather primordia (FPs). We show that different subsets of contiguous *Hoxd*
113 genes are expressed in the mouse VP mesoderm and in the chicken FP ectoderm, indicating an independent
114 co-option of *Hoxd* paralogs in these structures. While the transcription of these genes in VPs and FPs relies on
115 lineage-specific CREs located within different segments of the regulatory landscape, these CREs exploit a
116 largely conserved chromatin 3D architecture.

117 Our comparative analysis of the regulation at work during trunk extension also revealed that *Hoxd1*
118 displays an expression pattern markedly different from that of its neighboring paralogs, both in mouse and
119 chick, and that this *Hoxd1*-specific expression is driven by an evolutionary conserved CRE located in a region
120 predominantly interacting with *Hoxd1* in both species. However, the cis-regulatory code at work in the latter
121 regulation differs between the two species, illustrating the possibility that inter-species conservation of both
122 gene transcriptional specificity and chromatin architectures are compatible with a high plasticity of the *cis*-
123 regulatory sequences involved. The extension of this observation genome-wide suggests that conserved CRE
124 sequences more frequently diverge in their regulatory activities than they conserve their functionality.

## RESULTS

### Different *Hoxd* gene expression in mammalian and avian skin appendages.

We initially analyzed the expression profiles of *Hoxd* genes in mouse VPs and chicken FPs (Fig. 1). Skin appendage development starts with the interaction of the skin ectoderm with its underlying mesoderm, resulting in the thickening of the epithelium into a placode and in the condensation of dermal cells into a papilla (Mikkola, 2007; Sawyer and Knapp, 2003; Widelitz and Chuong, 1999). VP development starts at early embryonic day 12 (E12), forming a stereotyped array of eight columns and five rows of VPs (Wrenn and Wessells, 1984)(Fig. 1A). The epithelial placode subsequently invaginates and engulfs the dermal papilla forming the follicle primordium (Fig. S1). Likewise, in birds, ectoderm-mesoderm interactions result in the evagination of feather buds around embryonic day 7 (stage HH30-32 (Hamburger and Hamilton, 1951; Michon et al., 2007) (Fig. S2).

Whole-mount *in situ* hybridization (WISH) revealed strong *Hoxd1* expression in the dermal papillae of the VPs (Fig. 1B; Fig. S1). Furthermore, a comparative analysis of VPs from single E12.5 embryos revealed that *Hoxd1* transcripts accumulate slightly after ectodermal placode formation, marked by the expression of *Shh* (Chiang et al., 1999) (Fig. S1). *Hoxd3* and *Hoxd4* are also expressed in VPs, yet at much lower levels than *Hoxd1* (Fig. 1B, Fig. S1). Faint levels of *Hoxd8* mRNAs were sporadically detected in the VPs, while *Hoxd9* and more 5'-located *Hoxd* mRNAs were never observed in these structures (Fig. 1B, Fig. S1). *In situ* hybridization on cryostat sections confirmed that *Hoxd1* transcripts accumulate in the dermal mesenchyme of VPs, but not in the ectoderm-derived portion of the follicle (Fig. S1). Therefore, *Hoxd1-Hoxd4* are transcriptionally active in the dermal papillae of developing VPs, with *Hoxd1* being the main paralog expressed in these structures.

WISH experiments in HH35 chicken embryos revealed expression of *HOXD3*, *HOXD4, HOXD8* and *HOXD9* in the FPs, while *HOXD1* and *HOXD11* mRNAs were not detected (Fig. 1C, D, Fig S2). Cryostat sections indicated that *HOXD* gene expression in chicken FPs is localized in the follicle ectoderm (Fig. S2), in contrast with murine VPs. Different *Hoxd* genes thus operate in dermal papillae of mouse VPs and in ectodermal placodes of chicken FPs, likely reflecting the implementation of different regulatory mechanisms in the two lineages.

### *Hoxd* gene expression in the mouse and chicken embryonic body axis.

*Hox* genes are expressed in the paraxial and lateral mesoderm of the main embryonic axis, as well as in the neural tube, and display a progressively more restricted expression domain depending on their position within the cluster (Gaunt et al., 1988). Comparative WISH analysis of mouse and chicken embryos revealed that *Hoxd1* expression patterns in the trunk were markedly similar between the two species, yet largely divergent from that of the 5'-located neighbor *Hoxd* paralogs (Fig. 1E-G). While *Hoxd4* was strongly and

161 uniformly transcribed in the mouse paraxial and lateral mesoderm as well as in the neural tube, *Hoxd1*
162 displayed a biphasic expression pattern. Transcripts accumulated in the embryonic tailbud, yet they rapidly
163 disappeared from the presomitic mesoderm and remained undetected in lateral mesoderm progenitors or in the
164 neural tube (Fig. 1F). Instead, *Hoxd1* was specifically re-activated during somite condensation, coupling the
165 transcription of this gene to the segmentation clock (Dale and Pourquié, 2000; Zákány et al., 2001). Similar to
166 the mouse pattern, the chicken *HOXD1* expression also differed from its neighbouring paralogs, even though
167 its transcripts remained detectable in the formed somites all along the main body axis (Fig. 1G). These
168 observations suggested that *Hoxd1* transcription in developing somites may depend on a specific set of CREs,
169 different from CREs controlling the neighboring paralogs, and that this locus-specific transcription was
170 evolutionarily conserved across amniotes.
171
172 **An evolutionary conserved topology at the *HoxD* locus.**
173 In order to see whether these differences and similarities in regulatory specificities could be associated
174 to variations in the global chromatin architecture at this locus, we performed Capture Hi-C (CHi-C)
175 experiments using dissected mouse and chicken posterior trunks (Fig. 2A, B). Even though the global size of
176 TADs at this locus is approximately two times smaller in the chicken genome, the *HOXD* region closely
177 resembled its mouse counterpart, with the T-DOM being further organized into two sub-TADs in both species
178 (Fig. 2, sub-TAD1 and sub-TAD2) (Rodríguez-Carballo et al., 2020; Yakushiji-Kaminatsui et al., 2018). Of
179 note, the presence and relative distribution of conserved non-coding elements (CNEs) were maintained within
180 this similar chromatin architecture (Fig. 2, Fig. S3).
181 We corroborated these observations by assessing the interactions established by the *Hoxd1*, *Hoxd4*
182 and *Hoxd9* promoters in mouse and chicken embryonic posterior trunk cells, using 4C-seq (Fig. S3). As an
183 indication for non-tissue-specific interactions, we used embryonic brain cells where *Hox* genes are not
184 transcribed. In both species, the three viewpoints established frequent contacts with the T-DOM while
185 interactions with the C-DOM were virtually absent. In addition, all viewpoints contacted T-DOM sub-TAD1
186 with a higher probability than T-DOM sub-TAD2, showing specific and non-overlapping regions where
187 interactions were enriched. *Hoxd1* contacted the first half of sub-TAD1 (Figs. 3A and S3, region D1), more
188 intensively than *Hoxd4* or *Hoxd9* (Fig. S3). In turn, *Hoxd4* contacts within the 3' half of sub-TAD1 (Figs. 3A
189 and S3, region D4), were increased up to the sub-TAD boundary (Fig. S3). Finally, *Hoxd9* interactions were
190 mostly limited to the sub-TAD boundary region (Figs. 3A and S3, region D9), where they were higher than
191 for *Hoxd1* and *Hoxd4*. This distribution of interacting regions within the 3' TAD were found in both brain and
192 posterior trunk cells, yet with an overall lower contact frequency in brain cells, reflecting the transcription-
193 independent default conformation of the region, in agreement with previous reports (Andrey et al., 2013;
194 Dekker and Heard, 2015; Noordermeer et al., 2011).
195 Chromatin architectures partly rely upon the presence of the zinc-finger DNA binding protein CTCF,
196 which together with the cohesin complex can induce the formation and stabilization of large loops. (Hansen et

197 al., 2017; Nanni et al., 2020; Pugacheva et al., 2020). The ChIP-seq analysis of the CTCF profiles revealed
198 that both at the mouse and chicken *HoxD* loci, the telomeric end of the D1 region maps close to an occupied
199 CTCF site (Fig. S3, blue arrowhead). Also, a cluster of CTCF binding sites delimits the boundary between the
200 mouse and the chicken sub-TAD1 and sub-TAD2 (Rodriguez-Carballo et al., 2017; Rodríguez-Carballo et al.,
201 2020; Yakushiji-Kaminatsui et al., 2018) thus correlating with the limit between the *Hoxd4* and *Hoxd9*
202 interacting D4 and D9 regions in both species (Fig. 2; Fig. S3, blue arrowheads in panel B).
203 Overall, these results show that *Hoxd1*, *Hoxd4* and *Hoxd9* preferentially interact with different
204 portions of the T-DOM and that these segments are somehow determined by the distribution of CTCF binding
205 sites in T-DOM subTAD-1. These distinct interactions patterns are constitutive and conserved between mouse
206 and chicken. From these results, we concluded that the evolutionarily conserved contact topology of *Hoxd*
207 genes with T-DOM may contribute to the implementation of their specific regulatory strategies in mouse and
208 chicken embryonic structures.
209
210 **Tissue-specific regulatory sequences are located in regions of preferential interactions**
211 To evaluate whether the promoter-specific partition of contacts with T-DOM is associated with the
212 presence of differential regulatory activities, we set up to identify the CREs controlling *Hoxd* gene expression
213 in the VPs, FPs and the embryonic trunk of both mouse and chicken embryos. We carried out ChIP-seq
214 analyses using an antibody against H3K27ac, a histone modification indicative of an active chromatin state
215 (Creyghton et al., 2010; Rada-Iglesias et al., 2011) and annotated tissue-specific regions with increased density
216 of H3K27ac enrichment referred to as MARs (Most Acetylated Regions, Fig. 3). MARs were identified as
217 genomic regions accounting for the highest H3K27ac enrichment after subtraction of the corresponding signal
218 in brain cells (see material and methods).
219 In the mouse VPs, the MAR mapped within the D1 region (Fig. 3A, top, red-filled rectangle), in
220 agreement with the stronger expression of *Hoxd1* compared to its neighbouring paralogs (Fig. 1B; Fig. S1).
221 Instead, in chicken dorsal skin samples where *HOXD1* is not active (Fig. 1D), the MAR largely overlapped
222 the D4 and the D9 interacting regions (Fig. 3A, bottom, red-filled rectangle). Therefore, VPs and FPs display
223 different distributions of H3K27ac enrichment across T-DOM, in agreement with the various sibsets of *Hoxd*
224 gene expressed in these tissues. In contrast, the MARs of both mouse and chicken posterior trunk samples
225 largely overlapped the D4 region (Fig. 3B, red-filled rectangles) as expected from their similar expression
226 patterns in the embryonic trunk of both species, with the expression domain of *Hoxd4* being more extended
227 than that of *Hoxd9* (Fig. 1F). In summary, the different enrichments of H3K27ac marks across T-DOM were
228 located within the genomic segments that preferentially interacted with the genes expressed in each tissue.
229
230 ***Hoxd1* regulation in mutant regulatory landscapes**
231 To evaluate the functional importance of the D1 interacting region, we assessed *Hoxd1* transcription
232 in different mouse lines carrying mutations affecting this regulatory domain. We first analyzed *Hoxd1*

233 expression in the VPs of mouse embryos carrying various deletions of T-DOM (Fig. 4A, red lines). In the
234 *HoxD*$^{Del(attP\text{-}TpSB2)lac}$ allele, the D1 region is removed (hereafter referred to as *Del(attP-SB2)*. Since *Del(attP-*
235 *SB2)* homozygous embryos are not viable due to the deletion of the essential *Mtx2* gene (Andrey et al., 2013),
236 we crossed this line with the mouse line *HoxD*$^{Del(1\text{-}13)d9lac}$ (Spitz et al., 2001), hereafter referred to as *Del(1-13)*.
237 In the latter line, the entire *HoxD* cluster is deleted, such as to be able to see the effect of the *HoxD*$^{Del(attP\text{-}SB2)lac}$
238 deletion upon *Hoxd* gene regulation in *cis*. *Hoxd1* expression in the VPs of trans-heterozygous *HoxD*$^{Del(attP\text{-}}$
239 $^{TpSB2)lac/Del(1\text{-}13)}$ mutant embryos was completely abolished, in contrast with *Del(1-13)* heterozygous control
240 littermates (Fig. 4B). Conversely, the *HoxD*$^{Del(TpSB2\text{-}TpSB3)lac}$ allele (hereafter *Del(SB2-SB3)*(Andrey et al., 2013))
241 carries a large deletion that encompasses the whole T-DOM except the D1 region. We detected robust *Hoxd1*
242 expression in the VPs of E12.5 *HoxD*$^{Del(TpSB2\text{-}TpSB3)lac/Del(1\text{-}13)}$ trans-heterozygous mutant embryos (Fig. 4B).
243 We complemented these results by producing mouse transgenic embryos carrying bacterial artificial
244 chromosomes (BACs) spanning the *HoxD* cluster and/or parts of sub-TAD1 (in blue in Fig. 4A). In agreement
245 with the analysis of the T-DOM deletions, the BACs covering either the *HoxD* cluster (BAC$^{HoxD}$ (Schep et al.,
246 2016) or mapping outside of the D1 region (BAC$^{T1}$ (Delpretti et al., 2013) did not display any *lacZ* reporter
247 activity in E12.5 to E13.5 VPs (Fig. 4C). Instead, mouse embryos transgenic for BAC$^{Mtx2}$ (Allais-Bonnet et
248 al., 2021), which covers most of the D1 region, displayed strong reporter expression in the VPs (Fig. 4C).
249 Noteworthy, expression of *Hoxd1* was also abolished from facial mesenchymal progenitors in *Del(attP-SB2)*
250 mouse embryos, while it was reported by X-gal staining of BAC$^{Mtx2}$ transgenic embryos, illustrating that the
251 D1 region regulates the transcription of *Hoxd1* in several tissues.
252 To assess whether the D1 region is also necessary and sufficient for the specific *Hoxd1* expression
253 pattern in somites, we looked at *Hoxd1* transcription in posterior trunk cells using the same set of mutant
254 alleles. *Hoxd1* expression was abolished in developing somites of *Del(attP-SB2)* E9.5 embryos, compared to
255 their control *Del(1-13)* littermates (Fig. 4A, D), while similar transcript levels were maintained in the tailbuds,
256 suggesting that *Hoxd1* regulation in both structures involves different regulatory sequences. Accordingly,
257 embryos transgenic for BAC$^{Mtx2}$ displayed strong lacZ staining in somites but not in the tailbud, with stronger
258 activity in the last formed somites (Fig. 4A, E) thus closely mimicking native *Hoxd1* transcription in these
259 structures (Zákány et al., 2001). In contrast, *lacZ* expression was uniform along the paraxial mesoderm of
260 BAC$^{HoxD}$ transgenic embryos, yet without showing any *Hoxd1*-like specific reporter activity in the forming
261 somites. Altogether, these results confirmed the regulatory potential of the mouse D1 region for *Hoxd1*
262 expression patterns in facial tissues and in forming somites.
263
264 **Emergence of tissue-specific enhancers within conserved chromatin domains.**
265 *Hoxd1* transcription in VPs could have appeared through the evolution of a new CREs, in association
266 with the emergence of these structures in mammals. An alternative possibility would be the re-deployment of
267 a pre-existing element already at work in somites. The latter hypothesis comes from the fact that in both VPs
268 and somites, transcription of *Hoxd1* follows a cyclic dynamic, with a time progression in phase with the

269 production either of somites or of whisker pads. To address this question, we set up to isolate individual VP
270 enhancers and see if they would be active in somites. We generated two smaller BAC transgenes through
271 homologous recombination of a *lacZ* reporter construct, starting from BAC$^{Mtx2}$. While BAC$^{Mtx2a}$ displayed no
272 signal in VPs, BAC$^{Mtx2b}$ reported stable ß-galactosidase activity (Fig. S4A). Within the BAC$^{Mtx2b}$ region, three
273 candidate enhancers (ECs) were selected based on H3K27ac enrichment, one of them being also H3K27ac-
274 positive in posterior trunk cells (Fig. 4F, black and white arrowheads). Their regulatory potential was assessed
275 using transient *lacZ* reporter assays in transgenic mouse embryos and we identified a strong and reproducible
276 enhancer activity of *tgN*$^{EC1}$ in VPs, comparable to that observed in embryos transgenic for BAC$^{Mtx2}$ (Fig. 4G).
277 Instead, ß-galactosidase activity was not detected neither in *tgN*$^{EC2}$, nor in *tgN*$^{EC3}$ transgenic embryos (Fig.
278 S4B). We next tested these candidate enhancers at E9.5 to evaluate their regulatory potential in forming
279 somites. *EC2*, which was the only candidate sequence with significant H3K27ac enrichment in posterior trunk
280 cells, displayed reproducible activity in forming somites (Fig. 4H), unlike *tgN*$^{EC1}$ or *tgN*$^{EC3}$ (Fig. S4C). We
281 concluded that the only VP enhancer sequence identified was not active during somite formation, unlike a
282 somite enhancer located nearby (2.7 kb), within the D1 region.

283 The fact that two independent tissue-specific regulations rely on enhancers located in a close proximity
284 within a region of strong interactions suggests that a constrained topology may help the emergence of novel
285 regulatory sequence (Darbellay and Duboule, 2016b). To investigate how CREs might evolve within domains
286 of preferential interactions and how their activity might relate to the observed transcriptional outputs, we
287 compared our mouse and chicken H3K27ac datasets and WISH analyses with the percentage of DNA sequence
288 conservation. The number and distribution of putative CREs (pCREs, defined as non-coding H3K27ac peaks)
289 in the D1, D4 and D9 regions of both mouse and chicken were thus analyzed. Conserved non-coding sequences
290 (CNEs) were annotated by using blastz pairwise alignments downloaded from UCSC and from which all
291 elements overlapping with exons or promoters were discarded (Fig. S4D, E).

292 Overall, the number and distribution of pCREs in the different regions correlated with the
293 transcriptional activity of *Hoxd* genes. A majority of pCRE sequences did not coincide with CNEs, suggesting
294 a lineage-specific evolution of regulatory elements. Amongst those pCREs coinciding with CNEs, several
295 displayed regulatory activities in one species only (Fig. S4, black arrows) indicating a divergence in the
296 combinations of CREs at work, even in posterior trunk cells where the transcriptional activity is expected to
297 be similar in both species. This observation indicates that the sequence conservation of individual regulatory
298 elements is not an obligatory requirement to maintain similar transcription patterns.

299

300 **Divergent enhancer activities of conserved sequences.**

301 To take this analysis genome-wide, we compared the H3K27ac profiles across different mouse and
302 chicken embryonic tissues in relation to the presence of CNEs, by adding available proximal and distal
303 forelimb datasets (Beccari et al., 2016; Yakushiji-Kaminatsui et al., 2018) to our posterior trunk and skin
304 H3K27ac ChIP-seq datasets. pCREs were separated into putative enhancers and promoters, hereafter referred

305 to as ‘enhancers’ and ‘promoters’ for simplicity, with ‘enhancers’ mapping more than 2 kb away from a gene
306 transcription start site and ‘promoters’ mapping less than 2 kb away. pCREs which were H3K27ac-positive in
307 more than one of the analyzed tissues were categorized as ‘pleiotropic’ while those being active in only one
308 tissue were named ‘specific’ for the sake of classification. In both mouse and chicken, most promoters were
309 pleiotropic while the majority of enhancers were specific (Fig. 5A), a result in agreement with the usual
310 pleiotropic expression of genes carrying important developmental functions. When enhancers were divided
311 into ‘CNEs’ or ‘non-CNEs’, i.e. displaying or not sequence similarities between mouse and chicken, the
312 proportion of pleiotropic enhancers was higher amongst the former (Fig. 5A; p-value < e-15, Fisher test), an
313 increased level of sequence conservation that may reflect the higher evolutionary pressure on enhancers
314 endorsing multiple regulatory functions.

315 Next, we used CNEs to compare the regulatory activities of murine and chicken orthologous
316 sequences. In agreement with what was observed at the *HoxD* locus, the enhancer activities of CNEs, as
317 inferred by H3K27ac peaks, more often diverged than they matched between the related mouse and chicken
318 tissues (Fig. 5B, C). Hierarchical cluster analysis revealed that the enhancer profiles of CNEs were more
319 similar between different tissues of the same species, than between the same tissues in mouse and chicken
320 (Fig. 5B), a surprising observation as these CNEs were initially selected due to their sequence conservation
321 between the two species. We hypothesized that some sequences could have been kept over time despite a
322 divergence in their regulatory activities because they would endorse other functions in other tissues. To
323 evaluate this possibility, we represented on Euler diagrams the relationships between mouse and chicken CNEs
324 displaying enhancer features (Fig. 5C). Each mouse tissue was used as a reference in independent diagrams,
325 where chicken enhancer-CNEs were represented as different sets depending on whether they were active in
326 the same or in different tissues when compared to the mouse reference.

327 The intersection between the same tissue in mouse and in chicken represents elements that have both
328 a conserved sequence and regulatory function (Fig. 5C, overlaps circled in black). This intersection is smaller
329 than any difference between two sets, which indicates that DNA sequence similarity between two species can
330 be maintained amongst regulatory sequences despite divergences in their regulatory functions. We could
331 observe that CNEs often display enhancer activities in a chicken tissue that is different from the mouse tissue,
332 supporting this conclusion (Fig. 5C, overlaps circled in white). As a consequence, the regulatory activity of a
333 given sequence conserved between these two species cannot be used to predict its function(s) in the two
334 species.

335 Altogether, we show that both the global genomic organisation of the *HoxD* locus and specific domains
336 of preferential enhancer-promoter interactions are highly conserved between mouse and chicken. However,
337 the regulatory activities of individual CREs are largely species-specific and such sequences are systematically
338 found within those segments of regulatory landscapes that preferentially interact with the promoters of the
339 most highly transcribed genes. We also show that the lineage-specific evolution of regulatory activities could
340 either generate new regulatory relationships or, conversely, maintain ancestral transcription patterns.

341

342 **DISCUSSION**

343 **Versatile *Hoxd* gene functions in skin appendages.**

344 *Hox* genes play a dual role in skin appendage development. While their colinear expression is initially
345 necessary to pattern the skin dermis (Kanzler et al., 1997), they are subsequently transcribed in the dermal
346 papillae and/or ectoderm of embryonic and adult hair pelage follicles and vibrissae precursors (Godwin and
347 Capecchi, 1998; Packer et al., 2000; Reynolds et al., 1995; Yu et al., 2018), as well as in the avian buds
348 (Chuong et al., 1990; Kanzler et al., 1997). Here we show that the dermal papillae of embryonic mouse
349 vibrissae express *Hoxd1* to *Hoxd4*, with the former gene's mRNAs being the first detected, followed by
350 considerably lower levels of *Hoxd3* and *Hoxd4* RNAs. The transcription in VPs is driven by CREs located in
351 a region encompassing approximately 120kb of DNA adjacent to the telomeric end of the mouse *HoxD* cluster,
352 a region that is preferentially contacted by the *Hoxd1* gene. Therefore, a proximity effect is observed in the
353 building of a general chromatin architecture, based on constitutive contacts between the *Hoxd1* region and the
354 neighboring sub-TAD, whereby most of the *Hoxd1* regulatory sequences are located in the adjacent portion of
355 the regulatory landscape.

356 While a detailed functional characterization of *Hoxd* genes during the development of whiskers was
357 not the aim of this work, we did not observe any major morphological alteration in the vibrissae of mice
358 carrying genetic deletions of this precise region, despite the complete abrogation in the expression of *Hoxd1*
359 to *Hoxd4* in these structures. This lack of any visible abnormal phenotype may be due to functional redundancy
360 with other *Hox* paralogy groups expressed there, such as *Hoxc8* (Yu et al., 2018), to a lack of analytical power
361 or of the appropriate behavioral paradigms that may have revealed functionally abnormal whiskers. The
362 diverse expression of *Hox* paralogs in mammalian and avian skin appendages nonetheless illustrates the
363 plasticity in the usage of *Hox* gene functions in these structures. This plasticity likely relies upon the
364 independent acquisition of specific CREs for each gene cluster, as these skin derivatives emerged after the
365 genome duplication events thought to be at the origin of the vertebrate lineage (Holland et al., 2008; Holland
366 and Garcia-Fernàndez, 1996).

367 While *Hoxd9, Hoxd11* and *Hoxd13* are expressed in the ectoderm-derived hair fibers (Godwin and
368 Capecchi, 1998; Packer et al., 2000; Reynolds et al., 1995; Yu et al., 2018), we did not observe any *Hoxd1* in
369 the vibrissae shaft, nor any lacZ activity when the TgBAC$^{Mtx2}$ (carrying the D1 region) transgenics were used,
370 indicating that these expression patterns may depend on different sets of CREs. Our data also show that the
371 expression of *Hoxd3* to *Hoxd9* in the ectoderm of the chicken FPs depends on CREs unrelated to those
372 operating in the mouse VPs. These observations may indicate that different sets of *Hoxd* genes were
373 independently co-opted during the evolution of skin derivatives, likely through *de novo* enhancer acquisition
374 in the mammalian and avian lineages, in a way related to the regulation of *Hoxd9 and Hoxc13* in the embryonic
375 mammary buds and in the nails and hairs of mammals, respectively (Fernandez-Guerrero et al., 2020; Schep
376 et al., 2016). Alternatively, the rapid pace of tegument evolution in tetrapods may have been accompanied by

377 a divergence in enhancer sequences, which makes comparisons difficult. In this context, we can not rule out
378 the possibility that *Hoxd* gene regulation in skin appendages of both mammals and birds derives from an initial
379 pan-*Hoxd* expression pattern both in the ectoderm and mesoderm of skin appendages, which then evolved
380 differently in each lineage through modification of the CRE complement located within the adjacent TAD.
381 The fact that two CNEs acetylated in mouse VPs and chick FPs are also acetylated in mouse and chick posterior
382 trunk cells may indicate that the former structures co-opted parts of the regulatory mechanisms at work in the
383 latter. In this view, DNA sequence conservation may be due to constraints imposed by the function in the trunk
384 rather than by the function in the skin.
385
386 **Enhancer acquisition in evolving tetrapod skin appendages.**
387 TADs containing pleiotropic genes of key importance for vertebrate development are frequently
388 conserved across tetrapods and topological changes in their organization often correlate with important
389 modifications in gene expression (Eres et al., 2019; Liao et al., 2021; Torosin et al., 2020; Yakushiji-
390 Kaminatsui et al., 2018). Our results show that despite a considerable divergence in the non-coding elements
391 localized in the mouse and chicken T-DOM, the global pattern of interactions is conserved leading to similar
392 chromatin topologies. Indeed, in both cases, different *Hoxd* genes interact preferentially with distinct portions
393 of sub-TAD1. These contacts are for the most constitutive, even though we observed an activity-dependent
394 increase in interactions in the mouse VPs, and in mouse and chicken posterior trunk cells. Of interest, the
395 regions within T-DOM, which were preferentially contacted by the *Hoxd1*, *Hoxd4* or *Hoxd9* genes (D1 to D9)
396 are organized in a linear sequence opposite to the order of the genes themselves, as if *Hoxd1* was folding on
397 its closest possible chromatin environment within T-DOM, bringing along *Hoxd3* towards the next chromatin
398 segment and positioning the interactions involving *Hoxd9* further away into T-DOM. This sequential
399 positioning of interactions in mirror with spatial colinearity may impose a generic contact pattern, whereby
400 *Hoxd9*, for example, is unable to establish strong interactions with the D1 region and its enhancers, for this
401 region is primarily contacting *Hoxd1*, thus imposing constraints upon the distributions of interactions (see
402 below).
403 Furthermore, the distribution of H3K27ac-positive regions in the chicken FPs and mouse VPs across
404 these interacting regions correlate well with the specific subsets of *Hoxd* genes expressed in each of these
405 tissues. Finally, the regulation of *Hoxd1* in developing somites relies on evolutionary conserved elements
406 located in the region D1. This general regulatory topology is close to that observed in teleost fishes (Acemel
407 et al., 2016; Woltering et al., 2014), suggesting that it was already in place at the root of the vertebrate lineage
408 and that its hijacking by nascent enhancer sequences, may have favoured the co-option of specific *Hoxd* gene
409 subsets as targets of the novel regulations. The regulation of *Hoxd* genes in the mouse VPs and chicken FPs,
410 as well in the mouse mammary buds (Schep et al., 2016) may illustrate this process.
411
412 **Plasticity of the *cis*-regulatory code *versus* conservation in TAD organization.**

413 Due to their functional relevance in the regulation of gene expression, CREs tend to be evolutionarily
414 conserved across species (Sandelin et al., 2004; Sanges et al., 2013, 2006). However, several studies have
415 shown that enhancers controlling developmental gene expression can be functionally conserved even across
416 distant phylogenetic lineages despite a strong divergence in their DNA sequences (Ambrosino et al., 2019;
417 Berthelot et al., 2018; Wong et al., 2020) (Eichenlaub and Ettwiller, 2011; Schmidt et al., 2010; Villar et al.,
418 2015). Our inter-species comparison of CNEs enriched in H3K27ac across different embryonic structures
419 revealed that a considerable portion of evolutionary conserved CREs diverged in their patterns of activity
420 between the two species analyzed, in agreement with previous observations (Dermitzakis and Clark, 2002;
421 Schmidt et al., 2010; Vierstra et al., 2014; Villar et al., 2015). This dichotomy between the conservation of
422 enhancer sequences and their function is illustrated by the CREs controlling *Hoxd1* expression in the mouse
423 and chicken developing somites. While some of the sequences active in the mouse posterior trunk are
424 evolutionary and functionally conserved in chicken, such as EC2, which can drive lacZ expression in the last
425 formed somites of the murine embryo, other elements conserved at the nucleotide level displayed H3K27ac
426 enrichment only in the mouse.
427 In fact, a large fraction of H3K27ac-positive sequences detected either in the mouse or in the chicken
428 posterior trunk cells were not conserved between the two species, suggesting that they evolved in a species-
429 specific manner. In contrast, the high proportion of chicken promoters that display similar H3K27ac
430 enrichments in mice, together with the similar expression patterns observed for mouse and chicken *Hoxd* genes
431 in embryonic trunk cells, demonstrate that conserved gene expression can occur despite a high evolutionary
432 plasticity in the *cis*-regulatory code usage, in agreement with previous reports (Berthelot et al., 2018; Snetkova
433 et al., 2021). This may point to a regulatory strategy where multiple enhancers act coordinately to regulate the
434 same target gene(s) thus creating a quantitative effect in a way similar to the reported action of super-enhancers
435 (Sabari et al., 2018), yet where various subsets of CREs may display distinct tissue-specificities. This process
436 may be implemented preferentially within large regulatory landscapes, as e.g. in the case of *Fgf8* (Marinic et
437 al., 2013) or the TAD controlling *Hoxd* gene transcription in external genitals (Amândio et al., 2020).
438
439 **A regulatory playground with constraints.**
440 In those cases that were investigated, the respective positions of regulatory sequences within large
441 syntenic regulatory landscapes are generally conserved, and the global regulatory architecture found at one
442 particular developmental locus in one species can be extrapolated to its cognate locus in another amniote
443 species (e.g. (Kragesteen et al., 2018), implying that enhancer-promoter interactions are also evolutionary well
444 conserved, even for CREs acting over long distances (Irimia et al., 2012; Laverré et al., 2021), although some
445 mechanistic elements may vary (Ushiki et al., 2021). In agreement with this, and contrasting with the apparent
446 divergence in the *cis*-regulatory code controlling *Hoxd* gene expression in mouse and chicken embryos, our
447 phylogenetic footprinting and epigenetic analysis revealed that non-coding elements conserved in their DNA
448 sequence between the mouse and chicken genomes were distributed across the two species in a very similar

449 manner. Therefore, the potential gain and/or loss in the two lineages of particular CREs did not significantly
450 impact the internal organization of those conserved regulatory elements, nor did they impact upon the global
451 chromatin topology of the locus. This confirms the observation that even the significant divergence in CREs
452 located at the *HoxD* locus, which accompanied the evolution of the snake body plan, did not result in any
453 substantial alteration of the overall corn-snake *Hoxd* gene interaction map (Guerreiro et al., 2016). Altogether,
454 these observations suggest that the internal organization of the TADs at the *HoxD* locus and the specific
455 interaction profiles for various subsets of *Hoxd* target genes are resilient to considerable variation in their
456 CREs.

457 These results also highlight the somewhat dual properties that large regulatory landscapes may have
458 imposed in the course of regulatory evolution. On the one hand, a pre-established chromatin topology, as
459 materialized by TADs, may have provided unique 'structural niches' to evolve new enhancer sequences, due
460 to the proximity of factors already at work. This might especially apply to landscapes where a strong
461 quantitative parameter may be instrumental, and *a fortiori* when the target gene(s) are acting in combination,
462 coding for proteins of rather low specificities (Bolt and Duboule, 2020). This may be illustrated nowadays by
463 large landscapes, where all kinds of enhancer sequences are mixed within the same TAD. On the other hand,
464 this regulatory playground, while stimulating the emergence of regulations, will constrain their realms of action
465 due both to the very architecture that favors their evolution and to the accessibility to 'a' subset of contiguous
466 target genes as a result of the global distribution of interactions at this precise place of the landscape.

467

468 **MATERIAL AND METHODS**

469 **Mouse strains and chicken eggs**

470 All mutant strains are listed in Table S1 and were backcrossed continuously to Bl6/CBA mixed animals and
471 maintained as heterozygous stocks. Chick embryos from a White Leghorn strain were incubated at 37.5°C and
472 staged according to Hamburger and Hamilton (1951).

473 **Enhancer cloning and transgenic animals**

474 The different CRE candidate sequences were amplified using PCR-specific primers (see Table S2) and the
475 Expand High Fidelity PCR system (Roche). Amplified fragments were gel-purified and cloned into the pSK-
476 lacZ vector as in (Beccari et al., 2016). For the transgenesis assays, each lacZ reporter construct was digested
477 with NotI and KpnI and the restriction fragment encoding the potential enhancer sequence, the beta-globin
478 minimal promoter and the lacZ reporter gene was gel-purified and injected into the male pronucleus of
479 fertilized oocytes. F0 embryos were dissected either at E10, or at E12, fixed and stained for lacZ activity
480 according to standard protocols.

481 ***In situ* hybridization**

482 The probes used in this study for *in situ* hybridization were either previously reported, or produced by PCR
483 amplification of a fragment subsequently ligated in pGEMT Easy vector (Promega). Primers used to amplify

484 the fragment of interest are listed in Table S2. Digoxigenin (Dig) labeled probes were synthesized *in vitro* by
485 linearizing the respective plasmids using specific restriction enzymes and transcribed *in vitro* either with
486 T7/T3, or Sp6 RNA polymerase (Table S3) and the Dig-RNA labeling mix (Roche). The probes were purified
487 using the RNA easy mini kit. WISH experiments were performed as described in (Woltering et al., 2009).
488 Probes are listed in (Table S3). *In situ* experiments in sections were performed according to (Sockanathan and
489 Sockanathan, 2015). Cryostat sections were prepared after fixing embryos in 4% PFA solution at 4ºC
490 overnight. Subsequently, embryos were washed three times with PBS and passed to increasing sucrose
491 solutions at 4ºC in agitation (15% sucrose solution for 3-4 hours, followed by incubation in 30% sucrose
492 solution overnight) and finally included in OCT blocks. Sections of 20 µm were obtained with a Leica cryostat
493 and stored at -80ºC.

494 **ChIP-seq**

495 For genomics analyses, we used the mouse assembly mm10 and the chicken galGal6 and we plotted genomic
496 data with pyGenomeTracks 3.6 (Lopez-Delisle et al., 2021). ChIP-seq experiments were performed using the
497 ChIP-IT High sensitivity kit (active motif according to manufacturer instructions with minor modifications).
498 For the mouse samples, 12 pairs of E12.5 WPs, or one hundred E8.75 posterior trunks were used, the latter
499 dissected at the level of the 2$^{nd}$ to 4$^{th}$ pair of somites. For the chicken samples, the dorsal skin of five HH35
500 embryos or the posterior trunk or 80 HH19-21 posterior trunk regions were isolated. In all cases, the samples
501 were fixed for 10 min in 1% formaldehyde at RT and the crosslinking reaction was quenched with Glycine.
502 Subsequently, nuclei were extracted and sonicated in (Tris HCl pH 8.0 50mM, EDTA 10mM, 1% SDS ) to
503 an average fragment size of 200-500bp using a Diagenonode Bioruptor Sonicator. Ca. 10 to 20 µg of sonicated
504 chromatin were diluted tenfold with Dilution buffer (HEPES pH 7.3 20mM, EDTA 1mM, NaCl 150mM, NP40
505 0.1%) and incubated with 2 µg of anti-H3K27ac antibody (Abcam, ab4729). All buffers contained 1X
506 Complete Proteinase Inhibitor cocktail (EDTA-free; Roche) and 10mM Sodium Butyrate to prevent protein
507 degradation and Histone de-acetylation. Chromatin–antibody complexes were immunoprecipitated with
508 Protein G-coupled agarose beads-purified and de-crosslinked according to manufacturer instructions. Approx
509 5 to 10 ng of purified DNA were used for ChIP library preparation by the Geneva IGE3 Genomics Platform
510 (University of Geneva) and sequenced to obtain 100-bp single-end reads on an Illumina HiSeq2500 or
511 HiSeq4000 system. Published fastq files were downloaded from SRA for H3K27ac: mouse DFL
512 (GSM2713703, SRR5855214), mouse PFL (GSM2713704, SRR5855215), chicken DFL (GSM3182462,
513 SRR7288104), chicken PFL (GSM3182459, SRR7288101); and for CTCF in mouse PT (GSM5501395,
514 SRR15338248). ChIP-seq reads processing was done as in (Amândio et al., 2020) with some modifications,
515 using the laboratory Galaxy server (Afgan et al., 2016). Adapters and bad-quality bases were removed with
516 Cutadapt (v1.16.8) (Martin, 2011) (options -m 15 -q 30 -a
517 GATCGGAAGAGCACACGTCTGAACTCCAGTCAC). Reads were mapped to the mouse genome
518 (mm10) and to the chicken genome (galGla6) using Bowtie2 (v2.4.2) (Langmead and Salzberg, 2012)
519 with standard settings. Only alignments with a mapping quality >30 were kept (Samtools v1.13) (Danecek et

al. 2021). H3K27ac ChIP mapped reads were down sampled with Samtools view (v1.13) according to the sample with the smallest number of reads after filtering and duplicate removal (mouse: 71741225 reads; chicken 25872853 reads). Mouse CTCF ChIP mapped reads were down sampled with a fraction of 1/4 and chicken CTCF ChIP reads were not down sampled. When two replicates were available, alignment bam files were merged with Samtools merge (v1.13) and subsampled to the same number as single replicates. The coverage and peaks were obtained as the output of MACS2 (v2.1.1.20160309.6) (Zhang et al., 2008) with a fixed extension of 200 bp (--call-summits --nomodel --extsize 200 -B), and, for the WP sample, the q-value cutoff for peak detection was set to 0.1 instead of the 0.05 default. CTCF motif orientation was assessed using peaks extended by 100 bp each side and the CTCFBSDB 2.0 database (Ziebarth et al., 2012) with MIT_LM7 identified motifs.

**MAR annotation**

MARs are genomic segments of the T-DOM with the highest density of specific H3K27ac coverage and are annotated as follow: For mm10 chr2:74872605-75696338 and for galGal6 chr7:15856252-16252401, sliding windows are of 10 kb every 2 kb. For each window the coverage of the ChIP was computed and the difference with the coverage in the corresponding H3K27ac ChIP in the brain was considered as the specific signal. The smallest sequence of consecutive windows cumulating 30% (for the DS and WP samples) or 50% (for the PT samples) of the total specific signal is the MAR. See ChIP_scanRegionForHighestDensity_2files.py at https://gitlab.unige.ch/Aurelie.Hintermann/hintermannetal2022 for all details.

**pCREs**

pCREs are defined as genomic intervals that overlap with H3K27ac Macs2 peaks in at least one of the samples analyzed per species. To obtain the genomic coordinates of pCREs, Macs2 peaks of all samples were pooled into one file, the size of each peak was increased by 660 bp each side to account for nucleosome occupancy with bedtools slop (v2.30.0), and overlapping Macs2 peaks were combined into a single pCRE interval using bedtools merge. pCREs were annotated according to their colocalization with tissue-specific H3K27ac peaks, exons and sequence conservation using bedtools intersect. pCREs were quantified using R (v3.6.1) and the bar plots of Figure 5A were done with the ggplot2 package (v3.2.1). See CNEs_01.sh at https://gitlab.unige.ch/Aurelie.Hintermann/hintermannetal2022 for all details.

**CNEs**

Pairwise blastz alignments were downloaded from http://hgdownload.soe.ucsc.edu/goldenPath/mm10/vsGalGal6/mm10.galGal6.synNet.maf.gz and transformed to intervals with maf to interval (Blankenberg et al., 2011). Conserved elements were considered non-coding if they would not overlap with annotated exons neither in mouse nor in chicken. The synteny plot on Figure S3A was done using the R package ggplot2 (v3.2.1). CNEs were annotated according to their colocalization with tissue-specific H3K27ac peaks, exons and sequence conservation using bedtools intersect. pCREs were quantified using R (v3.6.1) and the bar plots of Figure 5A were done with the ggplot2 package (v3.2.1) (R Core Team (2019). R: A language and environment for statistical computing. R Foundation for

556 Statistical Computing, Vienna, Austria. URL https://www.R-project.org/.). The heatmap in Figure 5B was
557 done using the pheatmap R package (v1.0.12) using a matrix which columns are CNEs that overlapped with
558 an enhancer in at least one tissue in mouse or in chicken, rows are the tissues in which acetylation peaks were
559 called and values are the scores of acetylation peaks. If a CNE comprised several peaks of the same tissue, the
560 average was done. In Figure 5C, the relationships of the three sets formed by the conditions of being acetylated
561 in the mouse tissue, in the chicken tissue or in a chicken tissue excepted the one considered were represented
562 on Euler diagramms using the eulerr R package (v6.0.0), considering independently each tissue analyzed (i.e.
563 PT DFL PFL Skin and FB). See CNEs_01.sh at
564 https://gitlab.unige.ch/Aurelie.Hintermann/hintermannetal2022 for all details.

565 **4C-seq experiments**

566 4C-seq experiments were performed according to (Noordermeer et al., 2011). Briefly, the tissues were
567 dissected, dissociated with collagenase (Sigma Aldrich/Fluka) and filtered through a 35 microns mesh. Cells
568 were fixed with 2% formaldehyde (in PBS/10%FBS) for 10 min at RT and the reaction was quenched on ice
569 with Glycine. Nuclei were extracted using a cell lysis buffer (Tris pH 7.5 10 mM, NaCl 10 mM, $MgCl_2$ 5 mM,
570 EDTA 0.1 mM,) and stored at -80°C. Approximately 200 E9.5 posterior trunk regions dissected at the level of
571 the 2$^{nd}$ to 4$^{th}$ pair of somites, as well as 120 chicken HH19-21 posterior trunk samples, were used. Nuclei were
572 digested with NlaIII (New England Biolabs) and ligated with T4 DNA ligase HC (Promega) in diluted
573 conditions to promote intramolecular ligation. Samples were digested again with DpnII (New England
574 Biolabs) and re-ligated with T4 DNA ligase HC. These templates were amplified using Expand long template
575 (Roche) and PCR barcoded primers flanked with adaptors. For each library, 8 to 10 independent PCR reactions
576 were pooled together and purified using the PCR purification kit (Qiagen). Multiplexed libraries were
577 sequenced on Illumina HiSeq 2500 to obtain 100 bp single-end reads. Demultiplexing, mapping and 4C-seq
578 analysis were performed using a local version of the pipeline described in (David et al., 2014), on the mouse
579 mm10 and chicken galGal6 genome assemblies. The profiles were smoothened using a window size of 11
580 fragments and normalized to the mean score in +/-5 Mb around the viewpoint. When multiple independent
581 biological replicates were available, average 4C-seq profiles were calculated. When viewpoints were
582 subtracted, the score of each window of the normalized, smoothed profiles were subtracted (See
583 4C_subset_subtract at https://gitlab.unige.ch/Aurelie.Hintermann/hintermannetal2022) for all details.

584 **Capture Hi-C-seq experiments**

585 The SureSelectXT RNA probe design and capture Hi-C experiments were performed as described in (Bolt et
586 al., 2021b) for mouse and as in (Yakushiji-Kaminatsui et al., 2018) for chicken. Dissected tissues were
587 processed as in (Yakushiji-Kaminatsui et al., 2018) with the following changes: cells were cross-linked in 2%
588 formaldehyde/PBS and washed three times instead of being quenched by glycine. Hi-C-libraries were prepared
589 as in (Yakushiji-Kaminatsui et al., 2018). The first part of the data analysis was performed on our local galaxy
590 server (Afgan et al. 2016). Raw reads were preprocessed with CutAdapt (v1.16) (-a
591 AGATCGGAAGAGCACACGTCTGAACTCCAGTCAC -A

AGATCGGAAGAGCGTCGTGTAGGGAAAGAGTGTAGATCTCGGTGGTCGCCGTATCATT --minimum-length=15 --pair-filter=any --quality-cutoff=30) (Martin 2011). Then, Hicup (v0.6.1) (Langmead and Salzberg 2012; Dryden et al. 2014) and Samtools 1.2 (Danecek et al. 2021) were used with default parameters. The pairs were then loaded to 5-kb (mouse) and 2.5-kb (chicken) resolution matrices with Cooler v0.7.4 (Abdennur and Mirny 2020). These matrices were balanced with HiCExplorer hicCorrectMatrix (v3.7.2) using ICE as correction method, the mad threshold from HiCExplorer hicCorrectMatrix diagnostic plot as minimum threshold value and 5 as maximum threshold value. The TAD separation scores were computed with HiCExplorer hicFindTADs. (Ramírez et al. 2018; Wolff et al. 2020) with a fixed window of 240 kb in the mouse and 120 kb in the chicken. See CHiC_processRaws.sh https://gitlab.unige.ch/Aurelie.Hintermann/hintermannetal2022 for all details.

## ETHICS APPROVAL

All experiments involving animals were performed in agreement with the Swiss Law on Animal Protection (LPA), under license No GE 81/14 (to DD).

## DATA AVAILABILITY

All raw and processed datasets are available in the Gene Expression Omnibus (GEO) repository under accession number GSE195592. All scripts necessary to reproduce figures from raw data are available at https://gitlab.unige.ch/Aurelie.Hintermann/hintermannetal2022.

## COMPETING INTERESTS

The authors declare that they have no competing interests.


## FUNDING

This work was supported by funds from the University of Geneva, the Ecole Polytechnique Fédérale (EPFL, Lausanne), the Swiss National Research Fund (No. 310030B_138662) and the European Research Council grants System*Hox* (No 232790) and Regul*Hox* (No 588029) (to D.D.). Funding bodies had no role in the design of the study and collection, analysis and interpretation of data and in writing the manuscript.


## AUTHORS CONTRIBUTIONS

A. H. : Designed experiments, realized experiments and interpreted the results, wrote the manuscript

I. G. : Did some cloning and *in situ* hybridizations

C. C. B. : Provided unpublished datasets and helped for some the CHi-C experiments

L. L.-D.: Helped with the bioinformatic analyses

S. G. : Genotyped and helped analyze mouse mutants.

D. D. : Designed experiments, interpreted some results and wrote the paper.

L. B. : Designed experiments, interpreted some results and wrote the paper.

**ACKNOWLEDGEMENTS**

We thank all members of the Duboule laboratories for comments and discussions and Gregory Loichot for artwork. This work was supported in part by using the resources and services of both the Gene Expression Core Facility at the School of Life Sciences of the EPFL in Lausanne and the genomic platform from the IGE3 centre of the University of Geneva. Transgene injections were performed at the transgenesis platform of the University of Geneva Medical School.

**LEGENDS TO FIGURES**

**Figure 1. Transcription of *Hoxd* genes in mammalian and avian skin primordia. A.** Schematic illustration of a E12.5 mouse embryo with VPs (Vibrissae Primordia) represented as red circles. The dorso-ventral (D-V) and the caudo-rostral (C-R) axes are shown as red arrows representing the timing of appearance of the vibrissae primordia. **B.** WISH on E12.5 faces. The arrowheads point to the most caudo-dorsal placode, which is the largest one and the first to appear. Staining intensity progressively decreases from *Hoxd1* to *Hoxd8.* **C.** Schematic illustration of the back of a HH35 chicken embryo with feather placodes as red circles. A, anterior; P, posterior. **D.** WISH on HH35 chicken showing the skin of the upper back. The arrowheads point to the neck at the level of the shoulders. *HOXD1* is not expressed, whereas *HOXD3* and *HOXD8* signal intensities are stronger than for *HOXD4* and *HOXD9.* **E.** Schematic representation of a E9.5 or HH20 posterior trunk and tailbud. A, anterior; P, posterior; PSM, presomitic mesoderm; NT, neural tube; IM, intermediate mesoderm; FS, forming somites; PM, paraxial mesoderm; LM, lateral mesoderm; S, somites. **F.** WISH on E9.5 mouse posterior trunk and tail bud. *Hoxd1* transcription pattern is different from that of *Hoxd4* and *Hoxd9.* **G.** WISH on HH20 chicken posterior trunk and tail bud. *HOXD1* transcription pattern is different from *HOXD4* and *HOXD9.* The white arrowheads in panels **F** and **G** point to the *Hoxd1* stripe in the PSM. The black arrowheads show the difference between mouse (**F**) and chicken (**G**) in the *Hoxd1* mRNAs persistence in formed somites.

**Figure 2. Capture Hi-C-seq at the mouse and chicken *HoxD* loci. A**, **B.** Capture Hi-C-seq heatmaps using dissected posterior trunk cells. Below each heatmap, a CTCF ChIP-seq track is shown, produced from the same material. The similarities in the structural organization of the mouse and the chicken loci are underlined either by the positions of syntenic CNEs at key positions (numbered vertical dashed lines), the domains produced by TAD calling (black bars below) and the presence of a sub-TAD boundary (asterisk) within T-DOM. Genes are represented by empty rectangles. In panel **A,** E9.5 mouse posterior trunk cells were used and the CHi-C heatmap was mapped on mm10 with a bin size of 5 kb (chr2:73800000-75800000). In panel **B,** HH20 chicken posterior trunk cells were used and the CHi-C heatmap mapped on galGal6 with a bin size of

657 2.5kb (chr7:15790000-16700000) and on an inverted x-axis. The positions of the two TADs (T-DOM and C-
658 DOM) and of both sub-TADs are shown on top. The scales on the X axes were adjusted to comparable sizes
659 for ease of comparison, yet the chicken locus is more compacted (see the scale bars, bottom right).
660
661 **Figure 3. Tissue- and gene-specific interactions of dense H3K27ac regions. A.** On top is a ChIP-seq profile
662 of H3K27ac using mouse E12.5 VPs (orange) superimposed over the E12.5 forebrain cells (grey) (mm10,
663 chr2:73800000-75800000). Below is a H3K27ac profile produced from dissected chicken HH35 dorsal skin
664 (green), with HH18 brain cells (grey)(galGal6, chr7:15790000-16700000, inverted x-axis). The highest
665 interacting regions are depicted as D1, D4 and D9 (see also Figure S3B). The positions of conserved CNEs
666 were used to delimit these regions in both species (vertical dashed lines) and the extents of TADs are shown
667 below (thick black lines). The T-DOM (empty red rectangle) is split in overlapping genomic windows and the
668 densest window (Most Acetylated Region; MAR) is shown as a filled red rectangle. In the mouse VP, the
669 MAR is within the D1 DNA segment, whereas the chicken MAR overlaps with the D4 and D9 regions. **B.**
670 H3K27ac ChIP-seq using mouse E9.5 posterior trunk cells (orange) superimposed over forebrain cells
671 (grey)(mm10, chr2:73800000-75800000). Below is shown the H3K27ac profile obtained from the same
672 sample but dissected from a HH18 chicken embryo (green) with brain cells (grey) as a control (galGal6,
673 chr7:15790000-16700000, inverted x-axis). While the mouse posterior trunk Most Acetylated Region (MAR,
674 red rectangle) coincides with the D4 segment, the chicken MAR counterpart also covers D4 and a small part
675 of D9.
676
677 **Figure 4. Transcriptional regulation of *Hoxd1*. A.** The three deletion lines used are shown in red lines and
678 the transgenic BACs in blue lines. The extent of the D1 to D9 regions are shown on top (black) as well as the
679 positions of both sub-TADs below (thick black lines). **B.** WISH using a *Hoxd1* probe on E12.5 mouse embryos.
680 *Hoxd1* mRNAs were detected in both the control and the Del(SB2-SB3) lines (red arrowheads), yet the signal
681 was absent from Del(attP-SB2) mutant embryos (white arrowheads). **C.** X-gal staining on E12.5 mouse
682 embryos carrying randomly integrated BACs. A strong staining was detected in VPs when $BAC^{Mtx2}$ was used
683 (red arrowhead), whereas staining was not scored with the other two flanking BAC clones (white arrowheads).
684 Therefore, a region directly downstream the *HoxD* cluster is necessary and sufficient to activate *Hoxd1*
685 transcription in VPs, referred to as D1 region as it coincides with this previously defined region. **D.** WISH of
686 *Hoxd1* on E9.5 embryos focusing on tail buds. *Hoxd1* was detected in forming somites in both the control and
687 the *Del(SB2-SB3)* lines (red arrowheads), but was absent from *Del(attP-SB2)* mutant embryos (white
688 arrowhead). **E.** X-gal staining of E9.5 mouse embryos carrying various BAC transgenes. Staining was scored
689 in the entire neural tube and paraxial mesoderm with the $BAC^{HoxD}$ (black arrowhead). In contrast, embryos
690 carrying $BAC^{Mtx2}$ displayed staining in forming somites (red arrowhead), a staining absent when $BAC^{T1}$ was
691 used (white arrowhead). **F.** Enlargement of the D1 region along with a H3K27ac ChIP-seq using dissected
692 E12.5 VPs (orange, top) and E9.5 posterior trunk cells (orange, bottom) superimposed over E12.5 forebrain

693 (FB) cells (grey) (mm10; chr2:74747751-74916570). Above the profiles are the three VP acetylated elements
694 (black arrowheads) and below are MACS2 narrowPeaks for VPs and PTs (orange) and FB (grey). The position
695 of the three EC sequences used as transgenes (tgEC) are shown by numbered black boxes. **G.** X-gal staining
696 in VPs on a E12.5 embryo transgenic for *EC1*. **H.** X-gal staining in forming somites on E9.5 embryo transgenic
697 for the *EC2* sequence.
698
699 **Figure 5. Conserved sequences with divergent functions. A.** Bar plots showing the proportion of putative
700 *cis*-regulatory elements (pCREs) harbouring the H3K27ac mark in one ('specific') *versus* more than one
701 ('pleiotropic') tissues, in either mouse (orange) or chicken (green). For simplification purposes, distal pCREs
702 (>2kb away from the transcription start site) are referred as 'enhancers' and proximal pCREs (<2kb away from
703 transcription start site) are called 'promoters'. The different proportions are shown when comparing enhancers
704 and promoters (left), and conserved enhancers to non-conserved enhancers (right). The proportion of specific
705 *versus* pleiotropic elements is shown for CNEs and non-CNEs enhancers (right). In both mouse and chicken,
706 enhancers are more specific than promoters and amongst enhancers, conserved elements are found acetylated
707 in more tissues than non-conserved elements. **B.** Hierarchical clustering obtained using pheatmap R package.
708 On the *X*-axis are shown enhancer-CNEs i.e., conserved sequences, which are non-coding in mouse and in
709 chicken and which overlap with a H3K27ac mark in at least one species. On the *Y*-axis are displayed those
710 tissues used to obtain MACS2 processed peaks. The values on the heatmap correspond to the enrichment
711 scores of the peaks. Enhancer-CNEs cluster by species and not by tissues. **C.** Euler diagrams representing the
712 proportion of enhancer-CNEs, per tissue, acetylated in mouse (orange), in the corresponding chicken tissue
713 (dark green), or in unrelated chicken tissue (light green), showing that conserved sequence diverge in their
714 regulatory activities. The intersection between the same tissue in mouse and in chicken is delineated by a black
715 line, and the intersection between a chicken tissue different from the mouse tissue is delineated by a white line.
716 In **B.** and **C.** PFL, proximal forelimb; DFL, distal forelimb; posterior trunk, posterior trunk; DS, dorsal skin.
717
718 **LEGENDS TO SUPPLEMENTARY FIGURES**
719
720 **Supplementary Figure S1. Evolution of the *HoxD* locus and expression of *Hoxd* genes in the developing**
721 **VPs. A.** On the left is a schematic illustration of a vertebrate phylogenetic tree showing the emergence of some
722 skin derivatives (glands, scales, feathers, hairs). On the right are the corresponding versions of the *HoxD* locus,
723 with the orthologous *HoxD* gene clusters as shaded orange areas and other orthologous genes shown in green
724 to help delimit the extent of the conserved regulatory landscapes. **B.** Schematic representation of vibrissae
725 morphogenesis: epithelial placode (EP, yellow cells); dermal condensation (DC, blue cells). The approximate
726 developmental stage is indicated below, showing the delay between vibrissae and hair morphogenesis. The
727 dorsal skin of the upper back was used as reference for hairs. **C.** WISH on three successive E12 staged embryos
728 (indicated on the left) using four *Hoxd* genes as probes (top). The same three placodes are pointed by red

729 (positive) or white (negative) arrowheads. **D.** Schematic of the transversal section on E13.5 VPs (left),
730 analyzed in ISH with a *Hoxd1* probe (right). The scale bar in the right picture corresponds to 100 µm and the
731 *Hoxd1* stained VPs at peg stage (see below) are indicated by red arrowheads of decreasing intensities from left
732 to right. The staining is localized in dermal cells. **E.** WISH on E12.5 bisected mouse embryos. *Hoxd1* mRNAs
733 were detected after those for *Shh* (left) and before *Hoxd4* mRNAs (right).
734
735 **Supplementary Figure S2. Feather development and transcription of *Hoxd* genes. A.** Schematic of feather
736 development between stage HH20 and HH35 with ectodermal placode (EP, yellow) and dermal condensation
737 cells (DC, blue). **B.** WISH on HH35 chicken embryos, dorsal view of the upper back, with arrowheads pointing
738 toward the neck at the shoulder level. *HOXD11* transcripts were not detected in FPs (right), unlike those of
739 SHH (left). **C**. Transversal section through a HH35 chicken skin of the upper back (red), corresponding to the
740 two sections stained by ISH on the right. The scale bar is 100 µm. *SHH* is used as marker of the epithelial
741 placode (red arrowhead). *HOXD8* is also transcribed in epithelial placodes, matching -or slightly larger than-
742 the *SHH* domain.
743
744 **Supplementary Figure S3. Comparative 4C-seq analyses at the mouse and chicken *HoxD* loci. A.** Synteny
745 plots representing sequences conserved between the mouse and the chicken *HoxD* loci. On the X-axis is the
746 mouse locus (mm10, chr2:73800000-75800000) and on the Y axis is the chicken locus (galGal6,
747 chr7:15790000-16700000, inverted x-axis). The scale is the same for both axes. TADs and sub-TADs are
748 indicated by black lines and the *HoxD* cluster by a red rectangle. Schematic representations of the locus are on
749 top of each axis. Despite a mouse locus that is in average 2.2 times larger than its chicken counterpart, the
750 order of the conserved sequences is maintained, showing the absence of substantial genomic rearrangement at
751 this locus. **B**. On the Y axis are 4C-seq normalised scores per feature, with E9.5 mouse posterior trunk cells
752 scores (orange) superimposed over E12.5 FB cells (grey). Below the 4C tracks, the positions of the *Hoxd1,*
753 *Hoxd4* and *Hoxd9* viewpoints are represented by triangles, with a black triangle for the viewpoint used in the
754 track. Between each track, the subtraction of the two adjacent viewpoints is represented (black). The
755 preferentially interacting regions D1, D4 and D9 were annotated manually and, to facilitate comparisons
756 between their positions in the mouse and the chicken locus, orthologous CNEs located close to the edge of
757 each region D are shown (vertical dashed lines). CTCF ChIP-seq profiles are displayed below the 4C tracks,
758 with red and blue arrowheads below indicating their orientation. Color intensity is proportional to motif score.
759 Data mapped on mm10, chr2:73800000-75800000. **C.** On the Y axis are 4C-seq normalised scores per feature,
760 using HH18 chicken posterior trunk cells (green), superimposed with the profile obtained with HH18 brain
761 cells (grey). Data shown for *HOXD1* (top) *HOXD4* (middle) and *HOXD9* (bottom) viewpoints, with a black
762 arrowhead indicating the position of the viewpoint. Reads mapped on galGal6, chr7:15790000-16700000,
763 inverted x-axis.

764 **Supplementary Figure S4. Comparison of conserved and non-conserved CREs in mouse and chicken**
765 **embryonic tissues. A.** X-gal staining of E12.5 transgenic embryos carrying either the first half (left) or the
766 second half (right) of $BAC^{Mtx2}$. The entire $BAC^{Mtx2}$ recapitulated the pattern of expression of *Hoxd1* in VPs. **B.**
767 Staining of embryos carrying either the $TgN^{EC2}$ or the $TgN^{EC3}$ transgenes, which show no regulatory activity in
768 VPs at E12.5. **C.** Staining of E9.5 mouse embryos carrying the $TgN^{EC1}$ or the $TgN^{EC3}$ reporter constructs, which
769 show the absence of signal in forming somites. **D.** H3K27ac ChIP-seq profiles magnifications over the mouse
770 and chicken sub-TAD1. Top: Mouse E12.5 dissected VPs (orange) along with the mouse E12.5 forebrain cells
771 track (grey)(mm10, chr2:74775737-75222876). Below is the profile for the chicken HH35 dorsal skin (green),
772 superimposed to HH18 brain cells (grey) (galGal6, chr7:16033612-16252401, inverted x-axis). Processed
773 MACS2 narrowPeaks are in orange/green vertical lines and blastz conserved sequences in black vertical lines,
774 below each track. The peaks overlapping CNEs are pointed by black arrows. The peaks corresponding to CNEs
775 in both species and in equivalent tissues are pointed by red arrows. Vertical dashed lines represent the position
776 of corresponding CNEs at the edge of each region **E.** H3K27ac ChIP-seq focusing on sub-TAD1. Top: The
777 profile for mouse E9.5 posterior trunk cells (orange) are superimposed to mouse E12.5 forebrain cells (grey).
778 Bottom: Profiles of chicken HH18 embryonic posterior trunk cells (green) and of HH18 brain cells.

779 **LEGENDS TO SUPPLEMENTARY TABLES**

780
781 **Supplementary Table S1.** List of mouse lines
782
783 **Supplementary Table S2.** Primers used to clone candidate enhancer sequences
784
785 **Supplementary Table S3.** Probes for *in situ* hybridization
786
787

## BIBLIOGRAPHY


Acemel, R.D., Tena, J.J., Irastorza-Azcarate, I., Marlétaz, F., Gómez-Marín, C., de la Calle-Mustienes, E., Bertrand, S., Diaz, S.G., Aldea, D., Aury, J.-M., Mangenot, S., Holland, P.W.H., Devos, D.P., Maeso, I., Escrivá, H., Gómez-Skarmeta, J.L., 2016. A single three-dimensional chromatin compartment in amphioxus indicates a stepwise evolution of vertebrate Hox bimodal regulation. Nat. Genet. 48, 336–341. https://doi.org/10.1038/ng.3497

Afgan, E., Baker, D., van den Beek, M., Blankenberg, D., Bouvier, D., Čech, M., Chilton, J., Clements, D., Coraor, N., Eberhard, C., Grüning, B., Guerler, A., Hillman-Jackson, J., Von Kuster, G., Rasche, E., Soranzo, N., Turaga, N., Taylor, J., Nekrutenko, A., Goecks, J., 2016. The Galaxy platform for accessible, reproducible and collaborative biomedical analyses: 2016 update. Nucleic Acids Res. 44, W3–W10. https://doi.org/10.1093/nar/gkw343

Allais-Bonnet, A., Hintermann, A., Deloche, M.-C., Cornette, R., Bardou, P., Naval-Sanchez, M., Pinton, A., Haruda, A., Grohs, C., Zakany, J., Bigi, D., Medugorac, I., Putelat, O., Greyvenstein, O., Hadfield, T., Jemaa, S.B., Bunevski, G., Menzi, F., Hirter, N., Paris, J.M., Hedges, J., Palhiere, I., Rupp, R., Lenstra, J.A., Gidney, L., Lesur, J., Schafberg, R., Stache, M., Wandhammer, M.-D., Arbogast, R.-M., Guintard, C., Blin, A., Boukadiri, A., Rivière, J., Esquerré, D., Donnadieu, C., Danchin-Burge, C., Reich, C.M., Riley, D.G., Marle-Koster, E. van, Cockett, N., Hayes, B.J., Drögemüller, C., Kijas, J., Pailhoux, E., Tosser-Klopp, G., Duboule, D., Capitan, A., 2021. Analysis of Polycerate Mutants Reveals the Evolutionary Co-option of *HOXD1* for Horn Patterning in Bovidae. Mol. Biol. Evol. 38, 2260–2272. https://doi.org/10.1093/molbev/msab021

Amândio, A.R., Lopez-Delisle, L., Bolt, C.C., Mascrez, B., Duboule, D., 2020. A complex regulatory landscape involved in the development of mammalian external genitals. eLife 9, e52962. https://doi.org/10.7554/eLife.52962

Ambrosino, L., Vassalli, Q.A., D'Agostino, Y., Esposito, R., Cetrangolo, V., Caputi, L., Amoroso, A., Aniello, F., D'Aniello, S., Chatzigeorgiou, M., Chiusano, M.L., Locascio, A., 2019. Functional conserved non-coding elements among tunicates and chordates. Dev. Biol., Current Directions in Tunicate Development 448, 101–110. https://doi.org/10.1016/j.ydbio.2018.12.012

Andrey, G., Montavon, T., Mascrez, B., Gonzalez, F., Noordermeer, D., Leleu, M., Trono, D., Spitz, F., Duboule, D., 2013. A switch between topological domains underlies HoxD genes collinearity in mouse limbs. Science 340, 1234167. https://doi.org/10.1126/science.1234167

Beccari, L., Yakushiji-Kaminatsui, N., Woltering, J.M., Necsulea, A., Lonfat, N., Rodriguez-Carballo, E., Mascrez, B., Yamamoto, S., Kuroiwa, A., Duboule, D., 2016. A role for HOX13 proteins in the regulatory switch between TADs at the HoxD locus. Genes Dev. 30, 1172–1186. https://doi.org/10.1101/gad.281055.116

Belton, J.-M., McCord, R.P., Gibcus, J., Naumova, N., Zhan, Y., Dekker, J., 2012. Hi-C: A comprehensive technique to capture the conformation of genomes. Methods San Diego Calif 58. https://doi.org/10.1016/j.ymeth.2012.05.001

Berthelot, C., Villar, D., Horvath, J.E., Odom, D.T., Flicek, P., 2018. Complexity and conservation of regulatory landscapes underlie evolutionary resilience of mammalian gene expression. Nat. Ecol. Evol. 2, 152–163. https://doi.org/10.1038/s41559-017-0377-2

Biggs, L.C., Mikkola, M.L., 2014. Early inductive events in ectodermal appendage morphogenesis.

Blankenberg, D., Taylor, J., Nekrutenko, A., 2011. Making whole genome multiple alignments usable for biologists. Bioinformatics 27, 2426–2428. https://doi.org/10.1093/bioinformatics/btr398

Bolt, C.C., Duboule, D., 2020. The regulatory landscapes of developmental genes. Development 147, dev171736. https://doi.org/10.1242/dev.171736

Bolt, C.C., Lopez-Delisle, L., Mascrez, B., Duboule, D., 2021a. Mesomelic dysplasias associated with the HOXD locus are caused by regulatory reallocations. Nat. Commun. 12, 5013. https://doi.org/10.1038/s41467-021-25330-y

Bolt, C.C., Lopez-Delisle, L., Mascrez, B., Duboule, D., 2021b. MESOMELIC DYSPLASIAS ASSOCIATED WITH THE HOXD LOCUS ARE CAUSED BY REGULATORY REALLOCATIONS. bioRxiv 2021.02.01.429171. https://doi.org/10.1101/2021.02.01.429171

Bompadre, O., Andrey, G., 2019. Chromatin topology in development and disease. Curr. Opin. Genet. Dev. 55, 32–38. https://doi.org/10.1016/j.gde.2019.04.007

Carroll, S.B., 2008. Evo-Devo and an Expanding Evolutionary Synthesis: A Genetic Theory of Morphological Evolution. Cell 134, 25–36. https://doi.org/10.1016/j.cell.2008.06.030

Chiang, C., Swan, R.Z., Grachtchouk, M., Bolinger, M., Litingtung, Y., Robertson, E.K., Cooper, M.K., Gaffield, W., Westphal, H., Beachy, P.A., Dlugosz, A.A., 1999. Essential role for Sonic hedgehog during hair follicle morphogenesis. Dev. Biol. 205, 1–9. https://doi.org/10.1006/dbio.1998.9103

Chuong, C.M., Oliver, G., Ting, S.A., Jegalian, B.G., Chen, H.M., De Robertis, E.M., 1990. Gradients of homeoproteins in developing feather buds. Dev. Camb. Engl. 110, 1021–1030.

Creyghton, M.P., Cheng, A.W., Welstead, G.G., Kooistra, T., Carey, B.W., Steine, E.J., Hanna, J., Lodato, M.A., Frampton, G.M., Sharp, P.A., Boyer, L.A., Young, R.A., Jaenisch, R., 2010. Histone H3K27ac separates active from poised enhancers and predicts developmental state. Proc Natl Acad Sci USA 107, 21931–21936. https://doi.org/10.1073/pnas.1016071107

Dale, K.J., Pourquié, O., 2000. A clock-work somite. BioEssays 22, 72–83. https://doi.org/10.1002/(SICI)1521-1878(200001)22:1<72::AID-BIES12>3.0.CO;2-S

Darbellay, F., Bochaton, C., Lopez-Delisle, L., Mascrez, B., Tschopp, P., Delpretti, S., Zakany, J., Duboule, D., 2019. The constrained architecture of mammalian Hox gene clusters. Proc. Natl. Acad. Sci. U. S. A. 116, 13424–13433. https://doi.org/10.1073/pnas.1904602116

Darbellay, F., Duboule, D., 2016a. Chapter Sixteen - Topological Domains, Metagenes, and the Emergence of Pleiotropic Regulations at Hox Loci, in: Wassarman, P.M. (Ed.), Current Topics in Developmental Biology, Essays on Developmental Biology, Part A. Academic Press, pp. 299–314.

Darbellay, F., Duboule, D., 2016b. Topological Domains, Metagenes, and the Emergence of Pleiotropic Regulations at Hox Loci. Curr. Top. Dev. Biol. 116, 299–314. https://doi.org/10.1016/bs.ctdb.2015.11.022

David, F.P.A., Delafontaine, J., Carat, S., Ross, F.J., Lefebvre, G., Jarosz, Y., Sinclair, L., Noordermeer, D., Rougemont, J., Leleu, M., 2014. HTSstation: A Web Application and Open-Access Libraries for High-Throughput Sequencing Data Analysis. PLoS ONE 9, e85879. https://doi.org/10.1371/journal.pone.0085879

Dekker, J., Heard, E., 2015. Structural and functional diversity of Topologically Associating Domains. FEBS Lett. 589, 2877–2884. https://doi.org/10.1016/j.febslet.2015.08.044

Delpretti, S., Montavon, T., Leleu, M., Joye, E., Tzika, A., Milinkovitch, M., Duboule, D., 2013. Multiple enhancers regulate Hoxd genes and the Hotdog LncRNA during cecum budding. Cell Rep. 5, 137–50. https://doi.org/10.1016/j.celrep.2013.09.002

Dermitzakis, E.T., Clark, A.G., 2002. Evolution of Transcription Factor Binding Sites in Mammalian Gene Regulatory Regions: Conservation and Turnover. Mol. Biol. Evol. 19, 1114–1121. https://doi.org/10.1093/oxfordjournals.molbev.a004169

Dhouailly, D., 2009. A new scenario for the evolutionary origin of hair, feather, and avian scales. J. Anat. 214, 587–606. https://doi.org/10.1111/j.1469-7580.2008.01041.x

Dhouailly, D., Godefroit, P., Martin, T., Nonchev, S., Caraguel, F., Oftedal, O., 2019. Getting to the root of scales, feather and hair: As deep as odontodes? Exp. Dermatol. 28, 503–508. https://doi.org/10.1111/exd.13391

Di-Poï, N., Milinkovitch, M.C., 2016. The anatomical placode in reptile scale morphogenesis indicates shared ancestry among skin appendages in amniotes. Sci. Adv. 2, e1600708. https://doi.org/10.1126/sciadv.1600708

Dixon, J.R., Selvaraj, S., Yue, F., Kim, A., Li, Y., Shen, Y., Hu, M., Liu, J.S., Ren, B., 2012.

886 Topological domains in mammalian genomes identified by analysis of chromatin interactions.
887 Nature 485, 376–380.
888 Edwards, S.L., Beesley, J., French, J.D., Dunning, A.M., 2013. Beyond GWASs: Illuminating the
889 Dark Road from Association to Function. Am. J. Hum. Genet. 93, 779–797.
890 https://doi.org/10.1016/j.ajhg.2013.10.012
891 Eichenlaub, M.P., Ettwiller, L., 2011. De Novo Genesis of Enhancers in Vertebrates. PLoS Biol. 9.
892 https://doi.org/10.1371/journal.pbio.1001188
893 Eres, I.E., Luo, K., Hsiao, C.J., Blake, L.E., Gilad, Y., 2019. Reorganization of 3D genome
894 structure may contribute to gene regulatory evolution in primates. PLOS Genet. 15, e1008278.
895 https://doi.org/10.1371/journal.pgen.1008278
896 Fernandez-Guerrero, M., Yakushiji-Kaminatsui, N., Lopez-Delisle, L., Zdral, S., Darbellay, F.,
897 Perez-Gomez, R., Bolt, C.C., Sanchez-Martin, M.A., Duboule, D., Ros, M.A., 2020. Mammalian-
898 specific ectodermal enhancers control the expression of Hoxc genes in developing nails and hair
899 follicles. Proc. Natl. Acad. Sci. U. S. A. 117, 30509–30519.
900 https://doi.org/10.1073/pnas.2011078117
901 Gaunt, S., Sharpe, P.T., Duboule, D., 1988. Spatially restricted domains of homeo-gene transcripts
902 in mouse embryos: relation to a segmented body plan. Development 104 (suppl), 169–179.
903 Godwin, A.R., Capecchi, M.R., 1998. Hoxc13 mutant mice lack external hair. Genes Dev. 12, 11–
904 20.
905 Guerreiro, I., Gitto, S., Novoa, A., Codourey, J., Nguyen Huynh, T.H., Gonzalez, F., Milinkovitch,
906 M.C., Mallo, M., Duboule, D., 2016. Reorganisation of Hoxd regulatory landscapes during the
907 evolution of a snake-like body plan. eLife 5, e16087. https://doi.org/10.7554/eLife.16087
908 Hamburger, V., Hamilton, H.L., 1951. A series of normal stages in the development of the chick
909 embryo. J. Morphol. 88, 49–92. https://doi.org/10.1002/jmor.1050880104
910 Hansen, A.S., Pustova, I., Cattoglio, C., Tjian, R., Darzacq, X., 2017. CTCF and cohesin regulate
911 chromatin loop stability with distinct dynamics. eLife 6, e25776.
912 https://doi.org/10.7554/eLife.25776
913 Harmston, N., Ing-Simmons, E., Tan, G., Perry, M., Merkenschlager, M., Lenhard, B., 2017.
914 Topologically associating domains are ancient features that coincide with Metazoan clusters of
915 extreme noncoding conservation. Nat. Commun. 8. https://doi.org/10.1038/s41467-017-00524-5
916 Holland, L.Z., Albalat, R., Azumi, K., Benito-Gutiérrez, È., Blow, M.J., Bronner-Fraser, M.,
917 Brunet, F., Butts, T., Candiani, S., Dishaw, L.J., Ferrier, D.E.K., Garcia-Fernàndez, J., Gibson-
918 Brown, J.J., Gissi, C., Godzik, A., Hallböök, F., Hirose, D., Hosomichi, K., Ikuta, T., Inoko, H.,
919 Kasahara, M., Kasamatsu, J., Kawashima, T., Kimura, A., Kobayashi, M., Kozmik, Z., Kubokawa,
920 K., Laudet, V., Litman, G.W., McHardy, A.C., Meulemans, D., Nonaka, M., Olinski, R.P., Pancer,
921 Z., Pennacchio, L.A., Pestarino, M., Rast, J.P., Rigoutsos, I., Robinson-Rechavi, M., Roch, G.,
922 Saiga, H., Sasakura, Y., Satake, M., Satou, Y., Schubert, M., Sherwood, N., Shiina, T., Takatori, N.,
923 Tello, J., Vopalensky, P., Wada, S., Xu, A., Ye, Y., Yoshida, K., Yoshizaki, F., Yu, J.-K., Zhang,
924 Q., Zmasek, C.M., Jong, P.J. de, Osoegawa, K., Putnam, N.H., Rokhsar, D.S., Satoh, N., Holland,
925 P.W.H., 2008. The amphioxus genome illuminates vertebrate origins and cephalochordate biology.
926 Genome Res. 18, 1100–1111. https://doi.org/10.1101/gr.073676.107
927 Holland, P.W.H., Garcia-Fernàndez, J., 1996. HoxGenes and Chordate Evolution. Dev. Biol. 173,
928 382–395. https://doi.org/10.1006/dbio.1996.0034
929 Irimia, M., Tena, J.J., Alexis, M.S., Fernandez-Miñan, A., Maeso, I., Bogdanovic, O., de la Calle-
930 Mustienes, E., Roy, S.W., Gómez-Skarmeta, J.L., Fraser, H.B., 2012. Extensive conservation of
931 ancient microsynteny across metazoans due to cis-regulatory constraints. Genome Res. 22, 2356–
932 2367. https://doi.org/10.1101/gr.139725.112
933 Kanzler, B., Prin, F., Thelu, J., Dhouailly, D., 1997. CHOXC-8 and CHOXD-13 expression in
934 embryonic chick skin and cutaneous appendage specification. Dev. Dyn. Off. Publ. Am. Assoc.

Anat. 210, 274–287. https://doi.org/10.1002/(SICI)1097-0177(199711)210:3<274::AID-AJA8>3.0.CO;2-D

Kanzler, B., Viallet, J.P., Le Mouellic, H., Boncinelli, E., Duboule, D., Dhouailly, D., 1994. Differential expression of two different homeobox gene families during mouse tegument morphogenesis. Int. J. Dev. Biol. 38, 633–640.

Kragesteen, B.K., Spielmann, M., Paliou, C., Heinrich, V., Schöpflin, R., Esposito, A., Annunziatella, C., Bianco, S., Chiariello, A.M., Jerković, I., Harabula, I., Guckelberger, P., Pechstein, M., Wittler, L., Chan, W.-L., Franke, M., Lupiáñez, D.G., Kraft, K., Timmermann, B., Vingron, M., Visel, A., Nicodemi, M., Mundlos, S., Andrey, G., 2018. Dynamic 3D chromatin architecture contributes to enhancer specificity and limb morphogenesis. Nat. Genet. 50, 1463–1473. https://doi.org/10.1038/s41588-018-0221-x

Langmead, B., Salzberg, S.L., 2012. Fast gapped-read alignment with Bowtie 2. Nat Methods 9, 357–9. https://doi.org/10.1038/nmeth.1923

Laverré, A., Tannier, E., Necsulea, A., 2021. Long-range promoter-enhancer contacts are conserved during evolution and contribute to gene expression robustness. bioRxiv 2021.02.26.432473. https://doi.org/10.1101/2021.02.26.432473

Liao, Y., Zhang, X., Chakraborty, M., Emerson, J.J., 2021. Topologically associating domains and their role in the evolution of genome structure and function in Drosophila. Genome Res. 31, 397–410. https://doi.org/10.1101/gr.266130.120

Long, H.K., Prescott, S.L., Wysocka, J., 2016. Ever-Changing Landscapes: Transcriptional Enhancers in Development and Evolution. Cell 167, 1170–1187. https://doi.org/10.1016/j.cell.2016.09.018

Lopez-Delisle, L., Rabbani, L., Wolff, J., Bhardwaj, V., Backofen, R., Grüning, B., Ramírez, F., Manke, T., 2021. pyGenomeTracks: reproducible plots for multivariate genomic datasets. Bioinformatics 37, 422–423. https://doi.org/10.1093/bioinformatics/btaa692

Lupianez, D.G., Kraft, K., Heinrich, V., Krawitz, P., Brancati, F., Klopocki, E., Horn, D., Kayserili, H., Opitz, J.M., Laxova, R., Santos-Simarro, F., Gilbert-Dussardier, B., Wittler, L., Borschiwer, M., Haas, S.A., Osterwalder, M., Franke, M., Timmermann, B., Hecht, J., Spielmann, M., Visel, A., Mundlos, S., 2015. Disruptions of topological chromatin domains cause pathogenic rewiring of gene-enhancer interactions. Cell 161, 1012–25. https://doi.org/10.1016/j.cell.2015.04.004

Marinic, M., Aktas, T., Ruf, S., Spitz, F., 2013. An integrated holo-enhancer unit defines tissue and gene specificity of the Fgf8 regulatory landscape. Dev. Cell 24, 530–42. https://doi.org/10.1016/j.devcel.2013.01.025

Martin, M., 2011. Cutadapt removes adapter sequences from high-throughput sequencing reads. EMBnet.journal 17. https://doi.org/10.14806/ej.17.1.200

Michon, F., Charveron, M., Dhouailly, D., 2007. Dermal condensation formation in the chick embryo: Requirement for integrin engagement and subsequent stabilization by a possible Notch/integrin interaction. Dev. Dyn. 236, 755–768. https://doi.org/10.1002/dvdy.21080

Mikkola, M.L., 2007. Genetic basis of skin appendage development. Semin. Cell Dev. Biol., Mechanisms and biological significance of RNA localization AND Development of ectodermal appendages 18, 225–236. https://doi.org/10.1016/j.semcdb.2007.01.007

Montavon, T., Soshnikova, N., Mascrez, B., Joye, E., Thevenet, L., Splinter, E., de Laat, W., Spitz, F., Duboule, D., 2011. A Regulatory Archipelago Controls Hox Genes Transcription in Digits. Cell 147, 1132–1145. https://doi.org/10.1016/j.cell.2011.10.023

Nanni, L., Ceri, S., Logie, C., 2020. Spatial patterns of CTCF sites define the anatomy of TADs and their boundaries. Genome Biol. 21, 197. https://doi.org/10.1186/s13059-020-02108-x

Noordermeer, D., Leleu, M., Splinter, E., Rougemont, J., De Laat, W., Duboule, D., 2011. The dynamic architecture of Hox gene clusters. Science 334, 222–5. https://doi.org/10.1126/science.1207194

Nora, E.P., Lajoie, B.R., Schulz, E.G., Giorgetti, L., Okamoto, I., Servant, N., Piolot, T., van Berkum, N.L., Meisig, J., Sedat, J., Gribnau, J., Barillot, E., Bluthgen, N., Dekker, J., Heard, E., 2012. Spatial partitioning of the regulatory landscape of the X-inactivation centre. Nature 485, 381–5. https://doi.org/10.1038/nature11049

Packer, A.I., Jane-wit, D., McLean, L., Panteleyev, A.A., Christiano, A.M., Wolgemuth, D.J., 2000. Hoxa4 expression in developing mouse hair follicles and skin. Mech. Dev. 99, 153–157. https://doi.org/10.1016/S0925-4773(00)00471-8

Pantalacci, S., Chaumot, A., Benoît, G., Sadier, A., Delsuc, F., Douzery, E.J.P., Laudet, V., 2008. Conserved features and evolutionary shifts of the EDA signaling pathway involved in vertebrate skin appendage development. Mol. Biol. Evol. 25, 912–928. https://doi.org/10.1093/molbev/msn038

Pugacheva, E.M., Kubo, N., Loukinov, D., Tajmul, M., Kang, S., Kovalchuk, A.L., Strunnikov, A.V., Zentner, G.E., Ren, B., Lobanenkov, V.V., 2020. CTCF mediates chromatin looping via N-terminal domain-dependent cohesin retention. Proc. Natl. Acad. Sci. U. S. A. 117, 2020–2031. https://doi.org/10.1073/pnas.1911708117

Rada-Iglesias, A., Bajpai, R., Swigut, T., Brugmann, S.A., Flynn, R.A., Wysocka, J., 2011. A unique chromatin signature uncovers early developmental enhancers in humans. Nature 470, 279–283. https://doi.org/10.1038/nature09692

Rao, S.S.P., Huntley, M.H., Durand, N.C., Stamenova, E.K., Bochkov, I.D., Robinson, J.T., Sanborn, A.L., Machol, I., Omer, A.D., Lander, E.S., Aiden, E.L., 2014. A 3D Map of the Human Genome at Kilobase Resolution Reveals Principles of Chromatin Looping. Cell 159, 1665–1680. https://doi.org/10.1016/j.cell.2014.11.021

Rebeiz, M., Patel, N.H., Hinman, V.F., 2015. Unraveling the Tangled Skein: The Evolution of Transcriptional Regulatory Networks in Development. Annu. Rev. Genomics Hum. Genet. 16, 103–131. https://doi.org/10.1146/annurev-genom-091212-153423

Reid, A.I., Gaunt, S.J., 2002. Colinearity and non-colinearity in the expression of Hox genes in developing chick skin. Int. J. Dev. Biol. 46, 209–15. https://doi.org/10.1387/ijdb.011495

Reynolds, A.J., Lawrence, C.M., Jahoda, C.A., 1995. Hair follicle and fiber reconstruction. J. Invest. Dermatol. 104, 39S-40S. https://doi.org/10.1038/jid.1995.57

Rodríguez-Carballo, E., Lopez-Delisle, L., Willemin, A., Beccari, L., Gitto, S., Mascrez, B., Duboule, D., 2020. Chromatin topology and the timing of enhancer function at the HoxD locus. Proc. Natl. Acad. Sci. U. S. A. 117, 31231–31241. https://doi.org/10.1073/pnas.2015083117

Rodriguez-Carballo, E., Lopez-Delisle, L., Zhan, Y., Fabre, P.J., Beccari, L., El-Idrissi, I., Huynh, T.H.N., Ozadam, H., Dekker, J., Duboule, D., 2017. The HoxD cluster is a dynamic and resilient TAD boundary controlling the segregation of antagonistic regulatory landscapes. Genes Dev. 31, 2264–2281. https://doi.org/10.1101/gad.307769.117

Sabari, B.R., Dall'Agnese, A., Boija, A., Klein, I.A., Coffey, E.L., Shrinivas, K., Abraham, B.J., Hannett, N.M., Zamudio, A.V., Manteiga, J.C., Li, C.H., Guo, Y.E., Day, D.S., Schuijers, J., Vasile, E., Malik, S., Hnisz, D., Lee, T.I., Cisse, I.I., Roeder, R.G., Sharp, P.A., Chakraborty, A.K., Young, R.A., 2018. Coactivator condensation at super-enhancers links phase separation and gene control. Science 361. https://doi.org/10.1126/science.aar3958

Sandelin, A., Bailey, P., Bruce, S., Engström, P.G., Klos, J.M., Wasserman, W.W., Ericson, J., Lenhard, B., 2004. Arrays of ultraconserved non-coding regions span the loci of key developmental genes in vertebrate genomes. BMC Genomics 5, 99. https://doi.org/10.1186/1471-2164-5-99

Sanges, R., Hadzhiev, Y., Gueroult-Bellone, M., Roure, A., Ferg, M., Meola, N., Amore, G., Basu, S., Brown, E.R., De Simone, M., Petrera, F., Licastro, D., Strähle, U., Banfi, S., Lemaire, P., Birney, E., Müller, F., Stupka, E., 2013. Highly conserved elements discovered in vertebrates are present in non-syntenic loci of tunicates, act as enhancers and can be transcribed during development. Nucleic Acids Res. 41, 3600–3618. https://doi.org/10.1093/nar/gkt030

1033 Sanges, R., Kalmar, E., Claudiani, P., D'Amato, M., Muller, F., Stupka, E., 2006. Shuffling of cis-
1034 regulatory elements is a pervasive feature of the vertebrate lineage. Genome Biol. 7, R56.
1035 https://doi.org/10.1186/gb-2006-7-7-r56
1036 Sawyer, R.H., Knapp, L.W., 2003. Avian skin development and the evolutionary origin of feathers.
1037 J. Exp. Zoolog. B Mol. Dev. Evol. 298, 57–72. https://doi.org/10.1002/jez.b.26
1038 Schep, R., Necsulea, A., Rodríguez-Carballo, E., Guerreiro, I., Andrey, G., Nguyen Huynh, T.H.,
1039 Marcet, V., Zákány, J., Duboule, D., Beccari, L., 2016. Control of Hoxd gene transcription in the
1040 mammary bud by hijacking a preexisting regulatory landscape. Proc. Natl. Acad. Sci. U. S. A. 113,
1041 E7720–E7729. https://doi.org/10.1073/pnas.1617141113
1042 Schmidt, D., Wilson, M.D., Ballester, B., Schwalie, P.C., Brown, G.D., Marshall, A., Kutter, C.,
1043 Watt, S., Martinez-Jimenez, C.P., Mackay, S., Talianidis, I., Flicek, P., Odom, D.T., 2010. Five-
1044 Vertebrate ChIP-seq Reveals the Evolutionary Dynamics of Transcription Factor Binding. Science
1045 328, 1036–1040. https://doi.org/10.1126/science.1186176
1046 Sexton, T., Yaffe, E., Kenigsberg, E., Bantignies, F., Leblanc, B., Hoichman, M., Parrinello, H.,
1047 Tanay, A., Cavalli, G., 2012. Three-dimensional folding and functional organization principles of
1048 the Drosophila genome. Cell 148, 458–72. https://doi.org/10.1016/j.cell.2012.01.010
1049 Snetkova, V., Ypsilanti, A.R., Akiyama, J.A., Mannion, B.J., Plajzer-Frick, I., Novak, C.S.,
1050 Harrington, A.N., Pham, Q.T., Kato, M., Zhu, Y., Godoy, J., Meky, E., Hunter, R.D., Shi, M.,
1051 Kvon, E.Z., Afzal, V., Tran, S., Rubenstein, J.L.R., Visel, A., Pennacchio, L.A., Dickel, D.E., 2021.
1052 Ultraconserved enhancer function does not require perfect sequence conservation. Nat. Genet. 53,
1053 521–528. https://doi.org/10.1038/s41588-021-00812-3
1054 Sockanathan, S., Sockanathan, S., 2015. In situ hybridization of chick and mouse embryonic tissue.
1055 Protoc. Exch. https://doi.org/10.1038/protex.2015.040
1056 Spitz, F., Furlong, E.E.M., 2012. Transcription factors: from enhancer binding to developmental
1057 control. Nat. Rev. Genet. 13, 613–626. https://doi.org/10.1038/nrg3207
1058 Spitz, F., Gonzalez, F., Peichel, C., Vogt, T.F., Duboule, D., Zakany, J., 2001. Large scale
1059 transgenic and cluster deletion analysis of the HoxD complex separate an ancestral regulatory
1060 module from evolutionary innovations. Genes Dev 15, 2209–14.
1061 https://doi.org/10.1101/gad.205701
1062 Torosin, N.S., Anand, A., Golla, T.R., Cao, W., Ellison, C.E., 2020. 3D genome evolution and
1063 reorganization in the Drosophila melanogaster species group. PLOS Genet. 16, e1009229.
1064 https://doi.org/10.1371/journal.pgen.1009229
1065 Ushiki, A., Zhang, Y., Xiong, C., Zhao, J., Georgakopoulos-Soares, I., Kane, L., Jamieson, K.,
1066 Bamshad, M.J., Nickerson, D.A., University of Washington Center for Mendelian Genomics, Shen,
1067 Y., Lettice, L.A., Silveira-Lucas, E.L., Petit, F., Ahituv, N., 2021. Deletion of CTCF sites in the
1068 SHH locus alters enhancer-promoter interactions and leads to acheiropodia. Nat. Commun. 12,
1069 2282. https://doi.org/10.1038/s41467-021-22470-z
1070 Vierstra, J., Rynes, E., Sandstrom, R., Zhang, M., Canfield, T., Hansen, R.S., Stehling-Sun, S.,
1071 Sabo, P.J., Byron, R., Humbert, R., Thurman, R.E., Johnson, A.K., Vong, S., Lee, K., Bates, D.,
1072 Neri, F., Diegel, M., Giste, E., Haugen, E., Dunn, D., Wilken, M.S., Josefowicz, S., Samstein, R.,
1073 Chang, K.-H., Eichler, E.E., De Bruijn, M., Reh, T.A., Skoultchi, A., Rudensky, A., Orkin, S.H.,
1074 Papayannopoulou, T., Treuting, P.M., Selleri, L., Kaul, R., Groudine, M., Bender, M.A.,
1075 Stamatoyannopoulos, J.A., 2014. Mouse regulatory DNA landscapes reveal global principles of cis-
1076 regulatory evolution. Science 346, 1007–1012. https://doi.org/10.1126/science.1246426
1077 Villar, D., Berthelot, C., Aldridge, S., Rayner, T.F., Lukk, M., Pignatelli, M., Park, T.J., Deaville,
1078 R., Erichsen, J.T., Jasinska, A.J., Turner, J.M.A., Bertelsen, M.F., Murchison, E.P., Flicek, P.,
1079 Odom, D.T., 2015. Enhancer Evolution across 20 Mammalian Species. Cell 160, 554–566.
1080 https://doi.org/10.1016/j.cell.2015.01.006
1081 Widelitz, R.B., Chuong, C.M., 1999. Early events in skin appendage formation: induction of

1082 epithelial placodes and condensation of dermal mesenchyme. J. Investig. Dermatol. Symp. Proc.
1083 Soc. Investig. Dermatol. Inc Eur. Soc. Dermatol. Res. 4, 302–306.
1084 https://doi.org/10.1038/sj.jidsp.5640234
1085 Woltering, J.M., Noordermeer, D., Leleu, M., Duboule, D., 2014. Conservation and Divergence of
1086 Regulatory Strategies at Hox Loci and the Origin of Tetrapod Digits. PLoS Biol 12, e1001773.
1087 https://doi.org/10.1371/journal.pbio.1001773
1088 Wong, E.S., Zheng, D., Tan, S.Z., Bower, N.I., Garside, V., Vanwalleghem, G., Gaiti, F., Scott, E.,
1089 Hogan, B.M., Kikuchi, K., McGlinn, E., Francois, M., Degnan, B.M., 2020. Deep conservation of
1090 the enhancer regulatory code in animals. Science 370. https://doi.org/10.1126/science.aax8137
1091 Wu, P., Hou, L., Plikus, M., Hughes, M., Scehnet, J., Suksaweang, S., Widelitz, R., Jiang, T.-X.,
1092 Chuong, C.-M., 2004. Evo-Devo of amniote integuments and appendages. Int. J. Dev. Biol. 48,
1093 249–270. https://doi.org/10.1387/ijdb.041825pw
1094 Yakushiji-Kaminatsui, N., Lopez-Delisle, L., Bolt, C.C., Andrey, G., Beccari, L., Duboule, D.,
1095 2018. Similarities and differences in the regulation of HoxD genes during chick and mouse limb
1096 development. PLoS Biol. 16, e3000004. https://doi.org/10.1371/journal.pbio.3000004
1097 Yu, Z., Jiang, K., Xu, Z., Huang, H., Qian, N., Lu, Z., Chen, D., Di, R., Yuan, T., Du, Z., Xie, W.,
1098 Lu, X., Li, H., Chai, R., Yang, Y., Zhu, B., Kunieda, T., Wang, F., Chen, T., 2018. Hoxc-
1099 Dependent Mesenchymal Niche Heterogeneity Drives Regional Hair Follicle Regeneration. Cell
1100 Stem Cell 23, 487-500.e6. https://doi.org/10.1016/j.stem.2018.07.016
1101 Zákány, J., Kmita, M., Alarcon, P., de la Pompa, J.-L., Duboule, D., 2001. Localized and Transient
1102 Transcription of Hox Genes Suggests a Link between Patterning and the Segmentation Clock. Cell
1103 106, 207–217. https://doi.org/10.1016/S0092-8674(01)00436-6
1104 Zhang, Y., Liu, T., Meyer, C.A., Eeckhoute, J., Johnson, D.S., Bernstein, B.E., Nusbaum, C.,
1105 Myers, R.M., Brown, M., Li, W., Liu, X.S., 2008. Model-based analysis of ChIP-Seq (MACS).
1106 Genome Biol 9, R137. https://doi.org/10.1186/gb-2008-9-9-r137
1107 Ziebarth, J.D., Bhattacharya, A., Cui, Y., 2012. CTCFBSDB 2.0: a database for CTCF-binding sites
1108 and genome organization. Nucleic Acids Res. 41, D188–D194. https://doi.org/10.1093/nar/gks1165
1109

Hintermann et al.
Figure 1

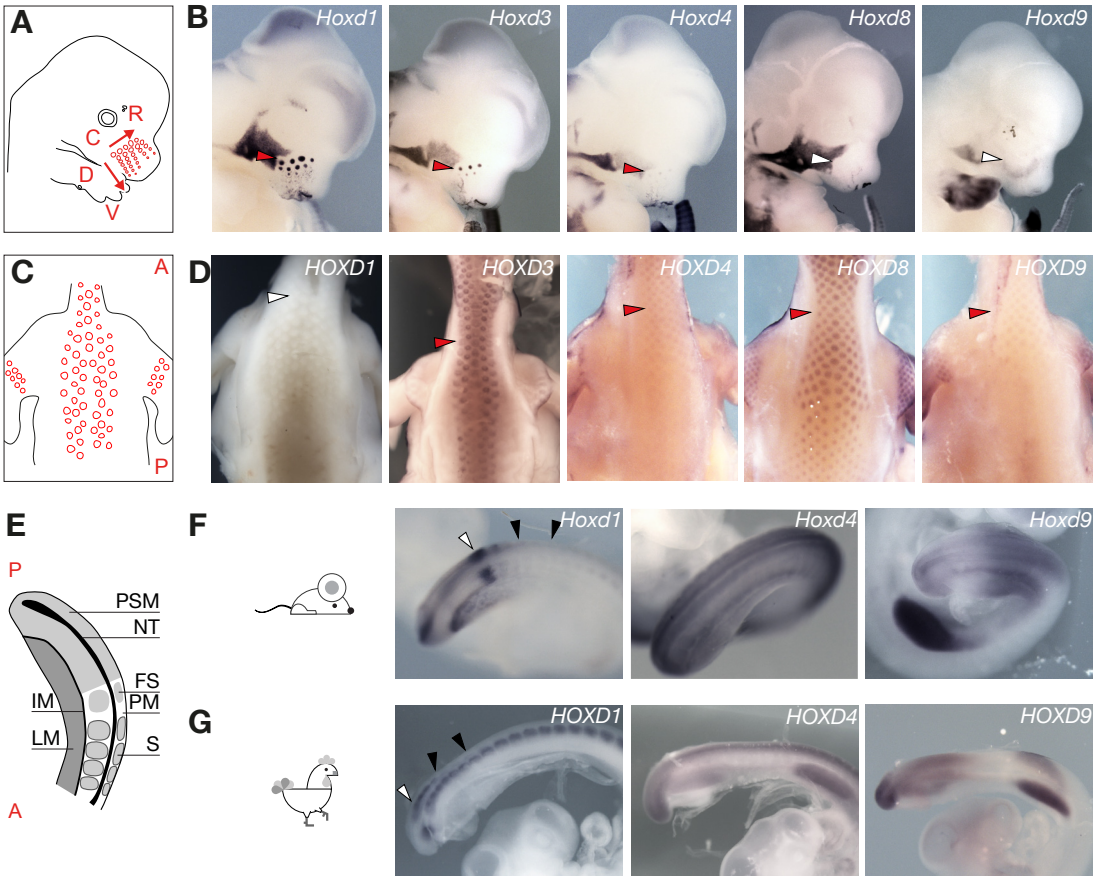

Hintermann et al.
Figure 2

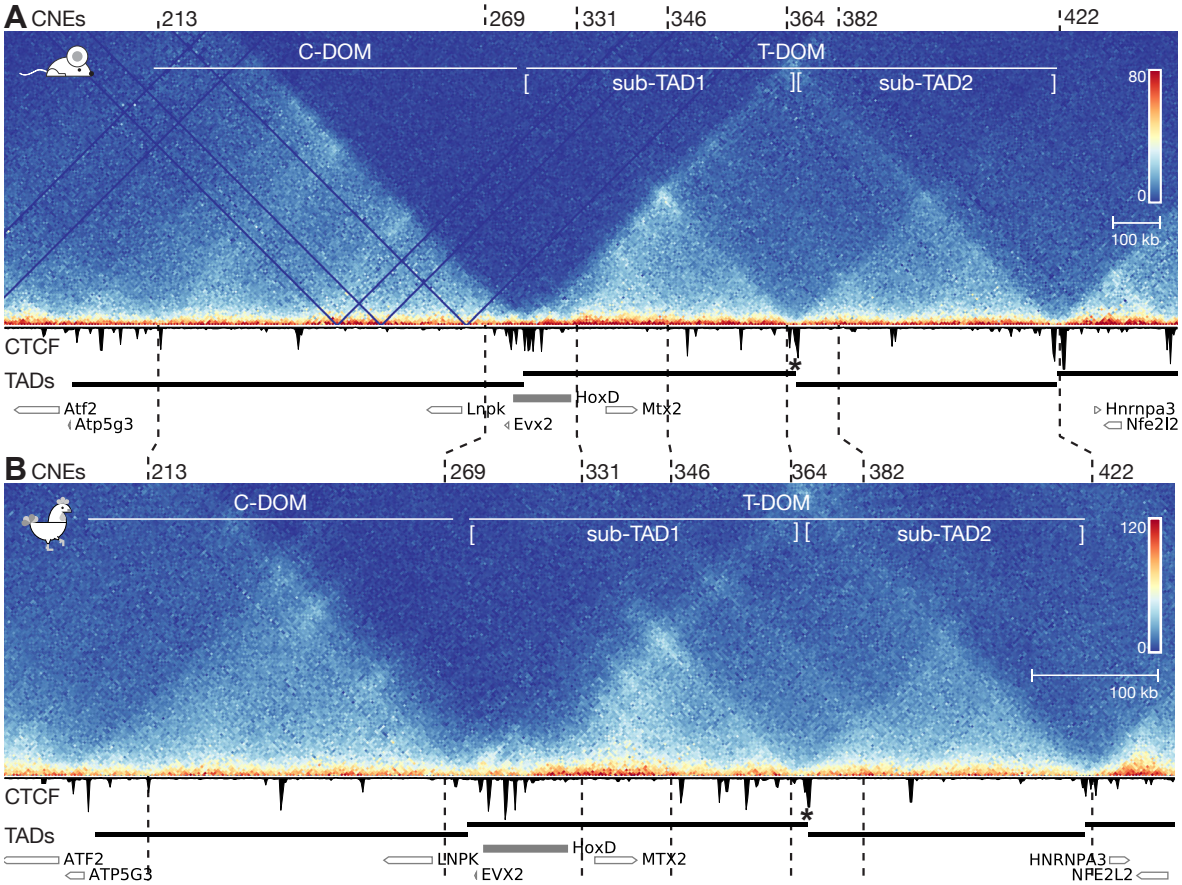

Hintermann et al.
Figure 3

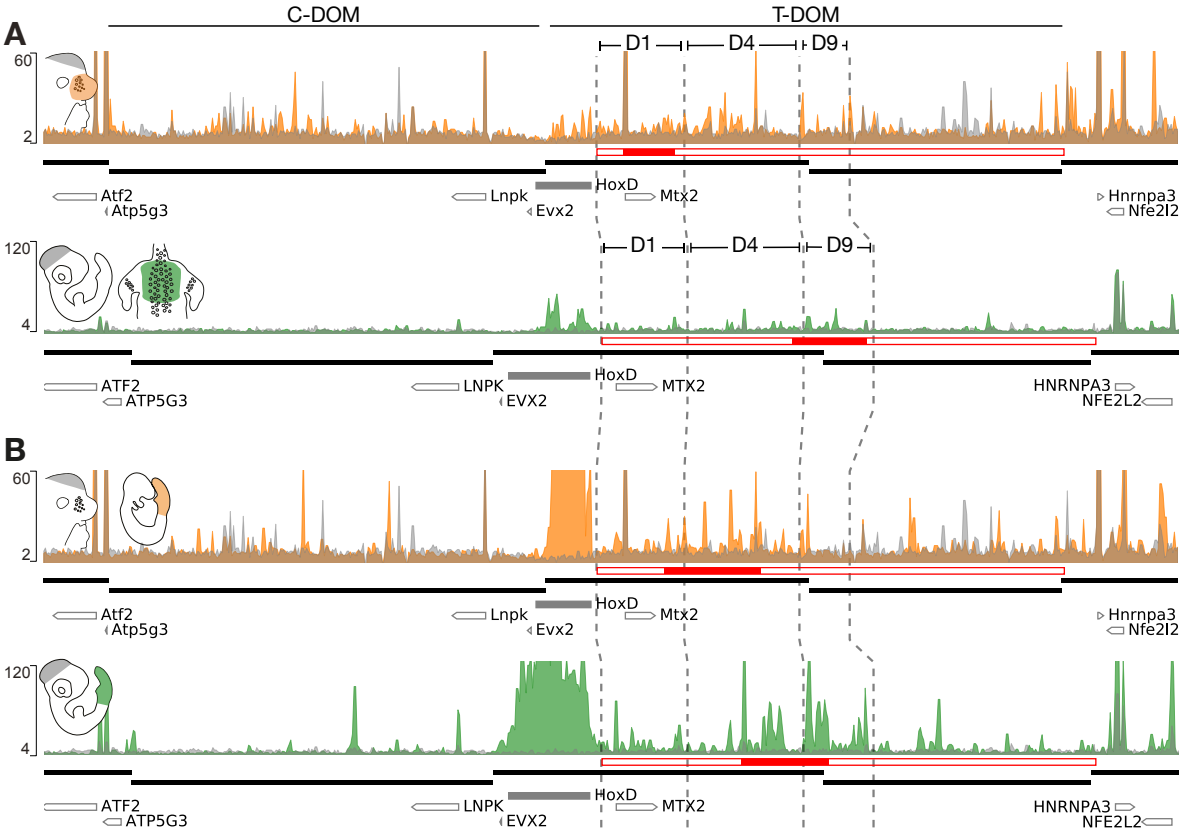

Hintermann et al.
Figure 4

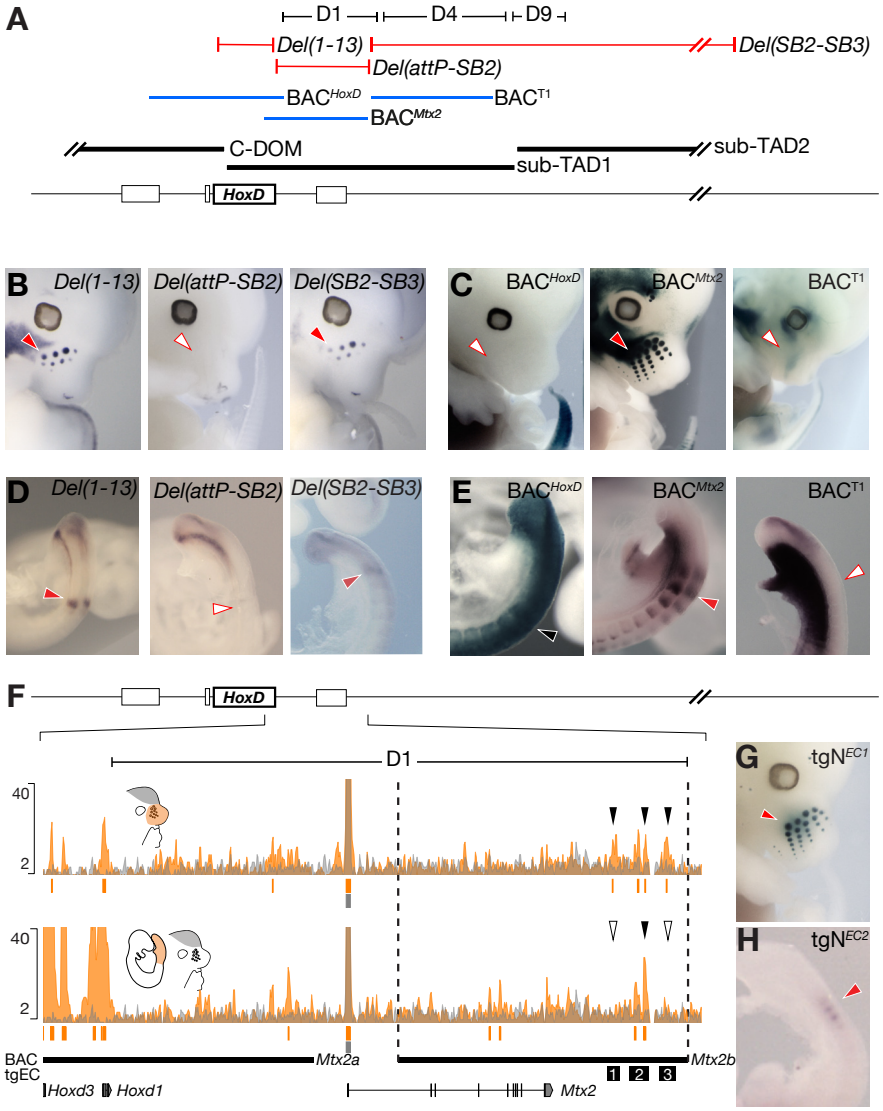

Hintermann et al.
Figure 5

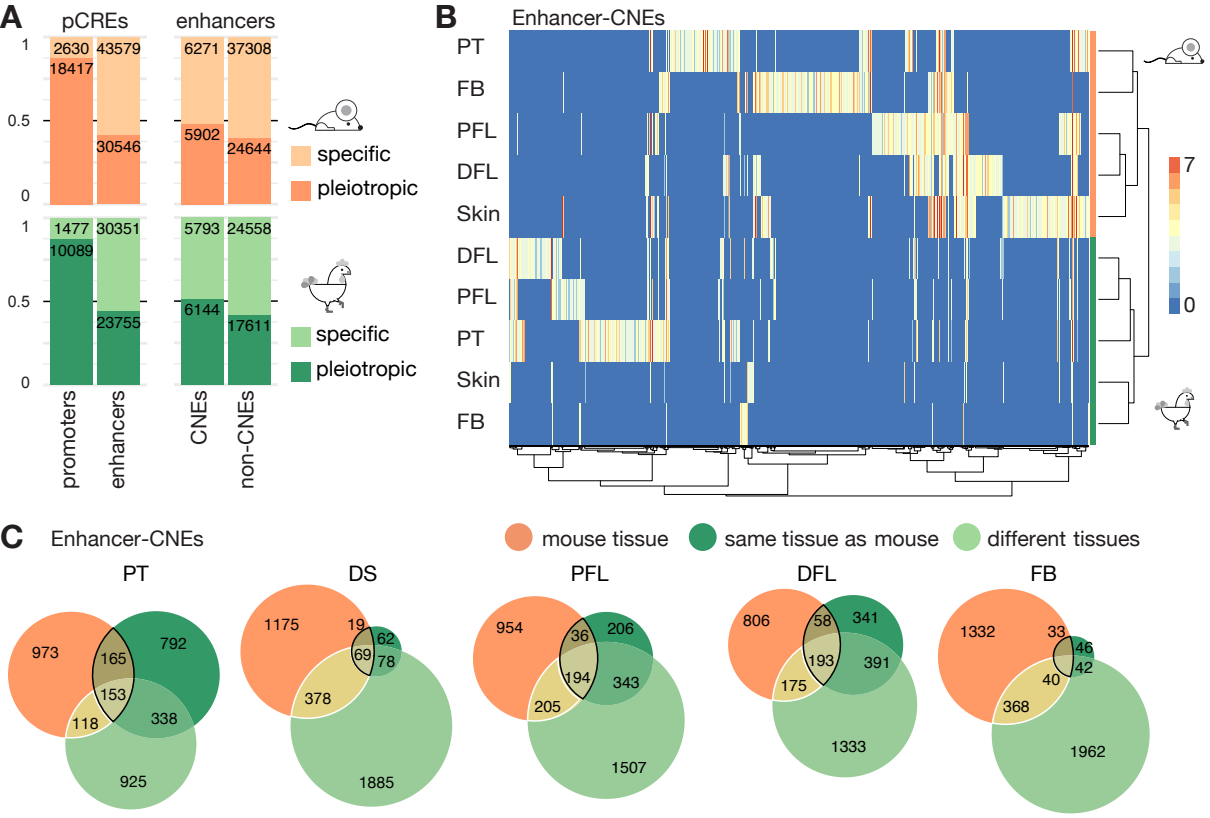

Hintermann et al.
Supplementary Figure S1

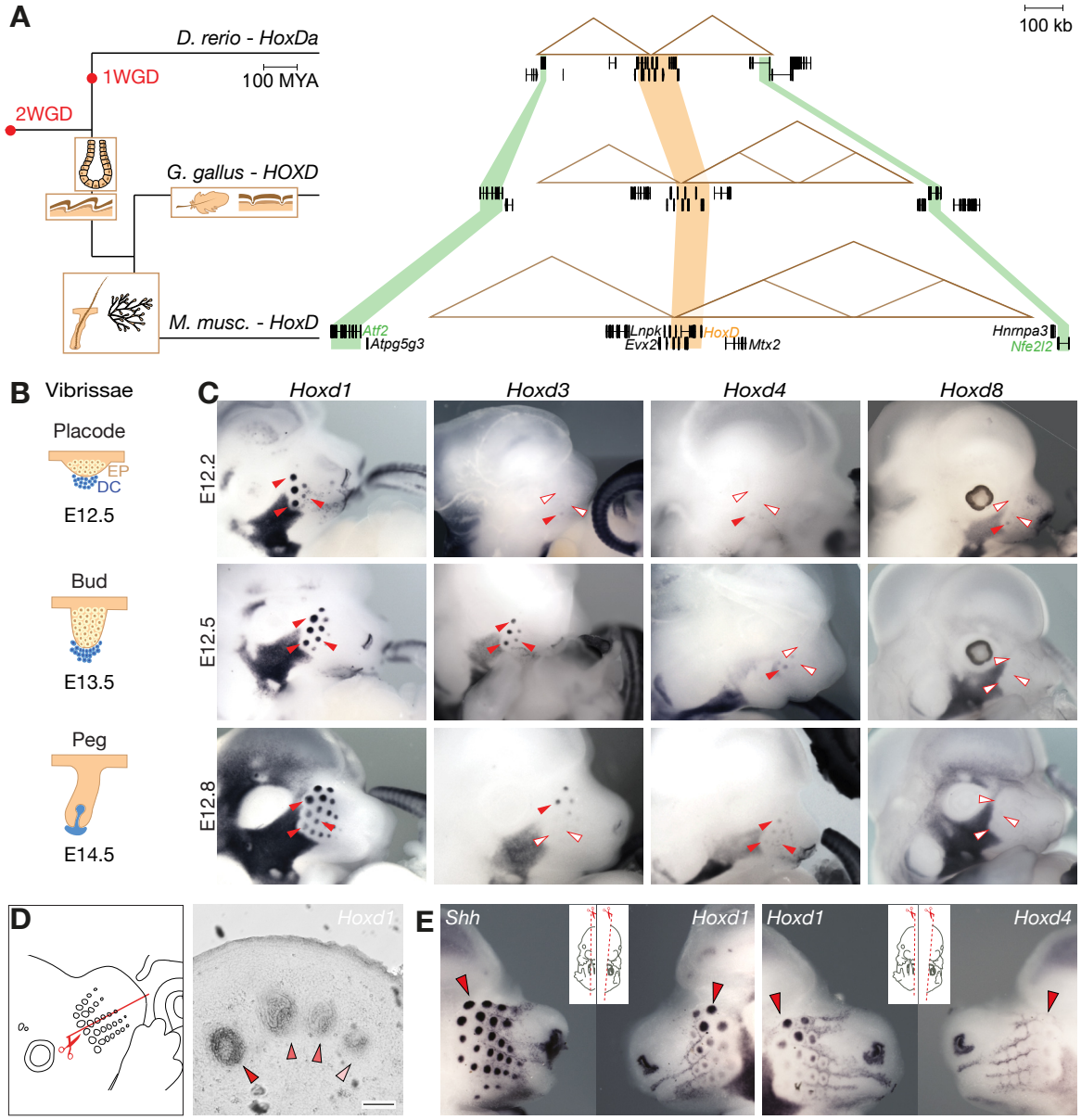

Hintermann et al.
Supplementary Figure S2

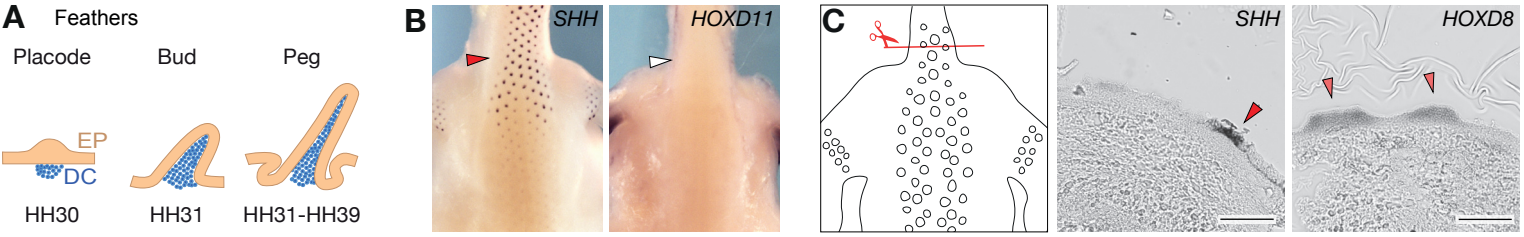

Hintermann et al.
Supplementary Figure S3

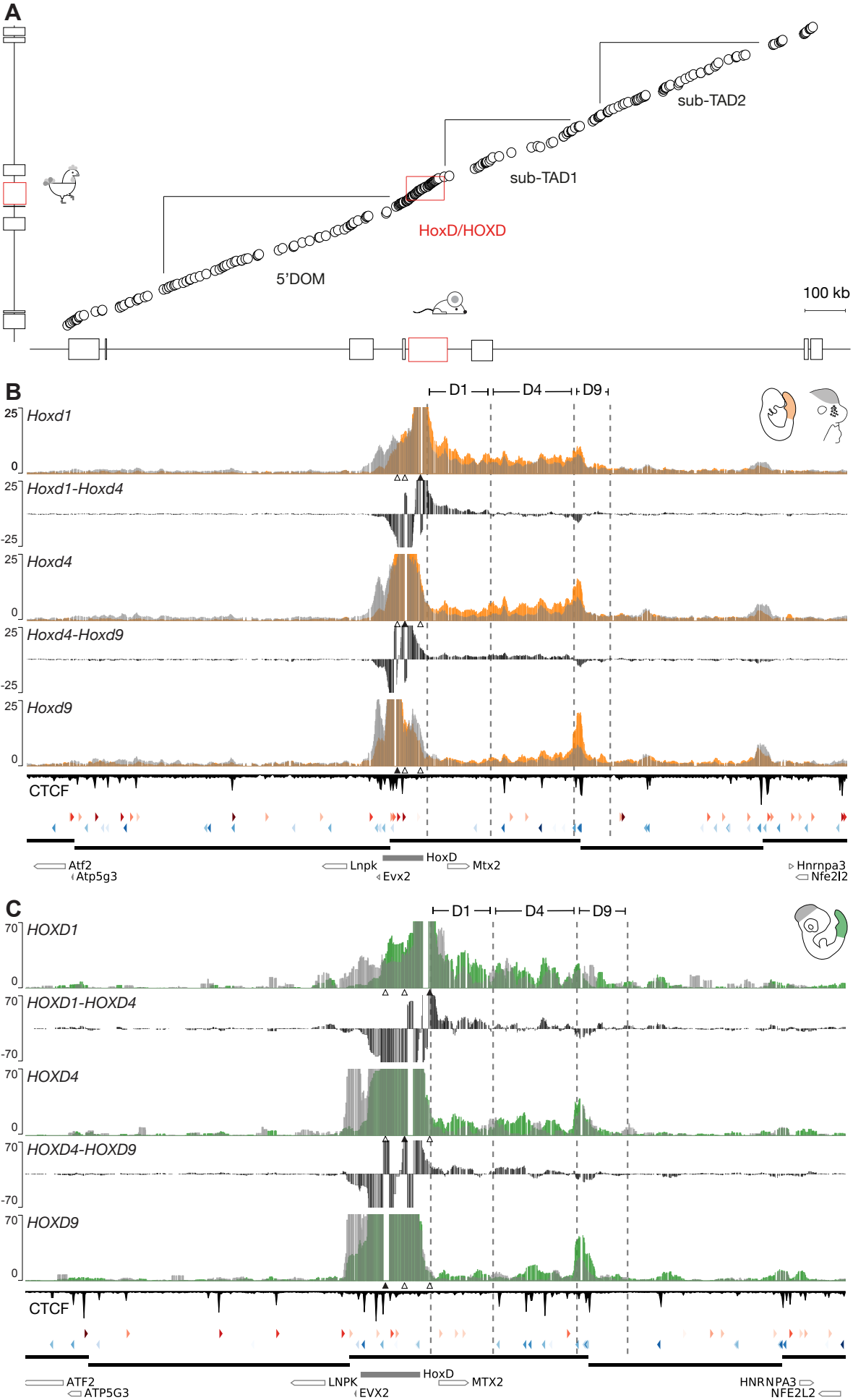

Hintermann et al.
Supplementary Figure S4

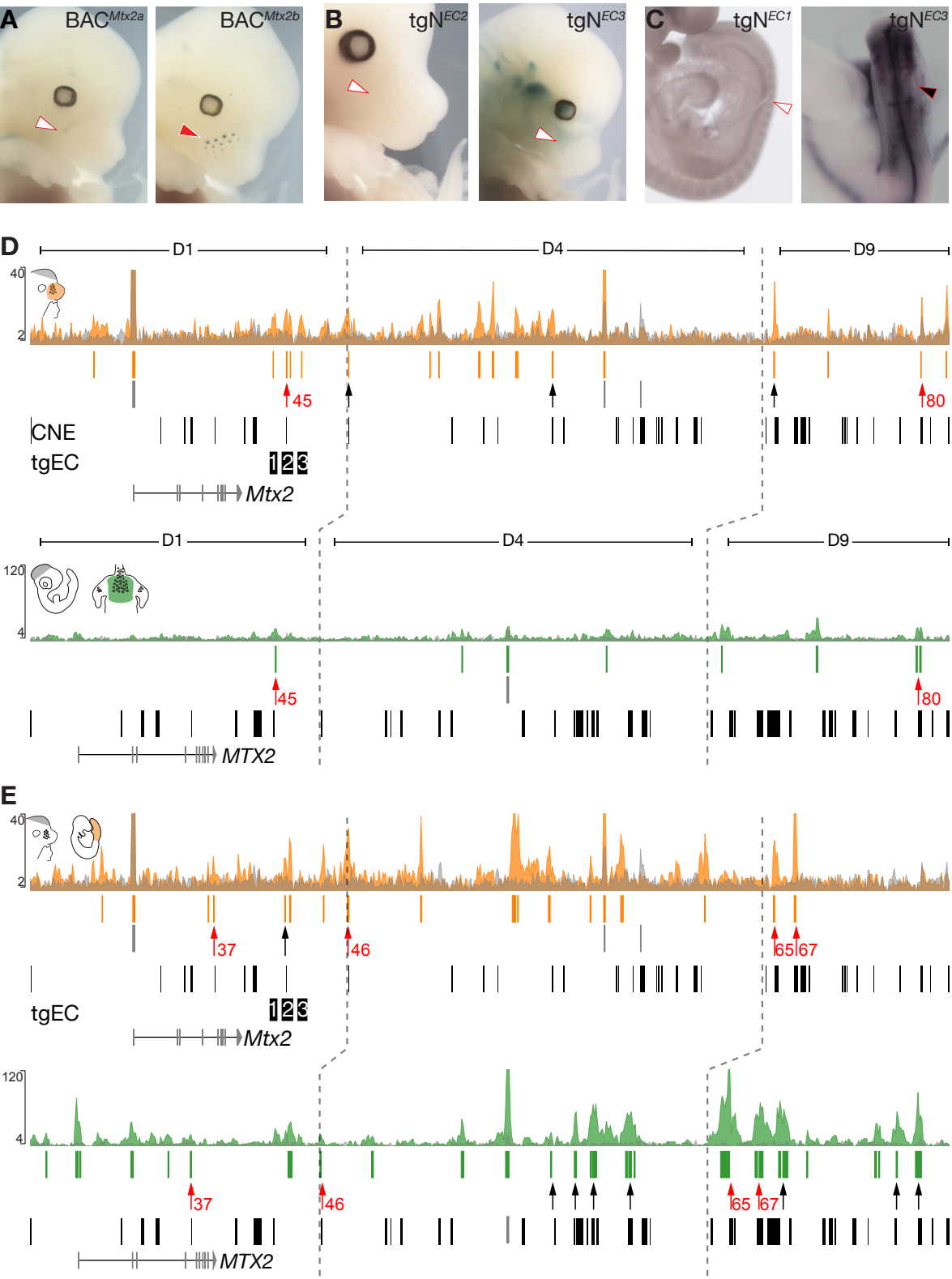

**Supplementary Table 1.** List of pre-existing modified mouse lines.

| Line | Reference | Coordinates | Primers for genotyping |
|---|---|---|---|
| Del(1-13)d9lac | (Rodriguez-Carballo et al., 2017) | chr2:74663889-74764314 | F : GACCGCTTATCCAATTCGGTTC<br>R : CAAGGTCCTCAGCCTTAAGAGTGG |
| Del(Attp-SB2) | (Andrey et al., 2013) | chr2:74765140-74916570 | F: ATCCCGGGGGATCCACTAGAG<br>R: GCTATATAGTAGTTT CAAGGCCAGCCC |
| Del(Attp-SB3) | (Andrey et al., 2013) | Chr2:74765140-75767350 | F: ATCCCGGGGGATCCACTAGAG<br>R: GCTTCCCTAGTTTATGGGGGAGG |
| Del(SB2-SB3) | (Schep et al., 2016) | chr2:74916560-75767350 | F: ATCCCGGGGGATCCACTAGAG<br>R: GCTTCCCTAGTTTATGGGGGAGG |
| TgBAC$^{Mtx2}$ | (Allais-Bonnet et al., 2021) | chr2:74747769-74913171 | F: CCTGCTGATGAAGCAGAACA<br>R: CAGCGACCAGATGATCACAC |
| TgBAC$^{T1}$ | BAC1 in (Delpretti et al., 2013) | chr2:74918538-75112340 | |
| TgBAC$^{T2}$ | BAC7 in (Delpretti et al., 2013) | chr2:75171805-75354437 | |
| TgBAC$^{HoxD}$ | (Schep et al., 2016) | chr2:74563168-74777972 | F: GGTAAACTGGCTCGGATTAGGG<br>R: CTATTCAAAGGTGGGGAGCAGTC |

**Supplementary Table 2.** Primers used to clone enhancer candidates.

| **CRE name** | **Coordinates** | **Primers for cloning** |
|---|---|---|
| EC1 | chr2:74892377-74895558 | F : TCCTCTCAAATTTTCCTAACCCCCA<br>R : CCCACCTGCCTCTACATAGCTC |
| EC2 | chr2:74898212-74903231 | F : CTGTCACCACCCCAGTCCTG<br>R : AAAAAGGGGGAGTGGGTGGG |
| EC3 | chr2:74905913-74910158 | F : AGGTTCCTGTCTTCGTGTTGG<br>R : GTAGCTCACCAGGGCTGAGG |

**Supplementary Table 3.** Probes for *In situ hybridization.*

Mouse

| Probe name | Reference | Digestion/ Transcription |
|---|---|---|
| *Hoxd1* | Our laboratory | NcoI / Sp6 |
| *Hoxd3* | Our laboratory | PmlI / T3 |
| *Hoxd4* | Our laboratory | EcoRI / Sp6 |
| *Hoxd8* | Our laboratory | EcoRI / T7 |
| *Hoxd9* | Our laboratory | BamHI / T7 |
| *Shh* | Our laboratory | HindIII / T7 |

Chicken

| Probe name / vector (size bp) | Reference | Digestion/ Transcription |
|---|---|---|
| *HOXD1* | Our laboratory | SalI / T7 |
| *HOXD3* | Our laboratory | SalI / T7 |
| *HOXD4* | Our laboratory | NcoI / Sp6 |
| *HOXD8* | Our laboratory | NotI / T3 |
| *HOXD9* | (Burke et al., 1995) | ClaI / T3 |
| *HOXD11* | (Burke et al., 1995) | EcoRI / Sp6 |
| *SHH* | Our laboratory | NcoI / Sp6 |

References

Allais-Bonnet, A., Hintermann, A., Deloche, M.-C., Cornette, R., Bardou, P., Naval-Sanchez, M., Pinton, A., Haruda, A., Grohs, C., Zakany, J., et al. (2021). Analysis of Polycerate Mutants Reveals the Evolutionary Co-option of *HOXD1* for Horn Patterning in Bovidae. *Molecular Biology and Evolution* 38, 2260–2272.

Andrey, G., Montavon, T., Mascrez, B., Gonzalez, F., Noordermeer, D., Leleu, M., Trono, D., Spitz, F. and Duboule, D. (2013). A switch between topological domains underlies HoxD genes collinearity in mouse limbs. *Science (New York, N.Y.)* 340, 1234167.

Burke, A. C., Nelson, C. E., Morgan, B. A. and Tabin, C. (1995). Hox genes and the evolution of vertebrate axial morphology. *Development* 121, 333–346.

Delpretti, S., Montavon, T., Leleu, M., Joye, E., Tzika, A., Milinkovitch, M. and Duboule, D. (2013). Multiple enhancers regulate Hoxd genes and the Hotdog LncRNA during cecum budding. *Cell reports* 5, 137–50.

Rodriguez-Carballo, E., Lopez-Delisle, L., Zhan, Y., Fabre, P. J., Beccari, L., El-Idrissi, I., Huynh, T. H. N., Ozadam, H., Dekker, J. and Duboule, D. (2017). The HoxD cluster

is a dynamic and resilient TAD boundary controlling the segregation of antagonistic regulatory landscapes. *Genes Dev* 31, 2264–2281.

Schep, R., Necsulea, A., Rodríguez-Carballo, E., Guerreiro, I., Andrey, G., Nguyen Huynh, T. H., Marcet, V., Zákány, J., Duboule, D. and Beccari, L. (2016). Control of Hoxd gene transcription in the mammary bud by hijacking a preexisting regulatory landscape. *Proc. Natl. Acad. Sci. U.S.A.* 113, E7720–E7729.